final report

Project code: B.GBP.0014

Prepared by: Dr Malcolm McPhee
NSW Department of Primary Industries
Dr Alen Alempijevic
UNIVERSITY OF TECHNOLOGY SYDNEY

Date published: 24 October 2017

PUBLISHED BY
Meat and Livestock Australia Limited
Locked Bag 1961
NORTH SYDNEY NSW 2059

Prototype on-farm 3D camera system to assess traits in Angus cattle

Meat & Livestock Australia acknowledges the matching funds provided by the Australian Government to support the research and development detailed in this publication.

Abstract

This project builds upon research carried out in a 'proof of concept' (B.BSC. 0339) study of 3D cameras to assess hip height, P8 fat and muscle score. The development of a 3D camera technology to assess live cattle has the potential to revolutionize the beef industry by providing real time objective measurements to assist producers ‘meet market specifications’ and put cash back in their pockets. Failing to ‘meet market specifications’ costs the beef industry $51M per year. In collaboration with the University of Technology Sydney we developed software and a portable measurement chute to demonstrate that hip height, P8 fat and muscle score can be accessed on live cattle within 15 seconds. The results from this study found that 70% of assessed P8 fat (n = 30) using the 3D camera technology lies within an accuracy of ± 1.5mm with a 97% repeatability across 4 sessions. The results also found that 77% of assessed muscle score (n = 30) using the 3D camera technology lies within an accuracy of ± 1 on a 15 point scale with an 80% repeatability across 4 sessions. The 3D technology reduces the variability across assessors and would be a one off cost providing a quick return for investment.

Executive summary

Why the work was done
This project builds upon research work carried out in a 'proof of concept' (B.BSC. 0339) study of 3D comers to assess hip height, P8 fat and muscle score and a pasture fed compliance project (B.SBP.0108) assessing market specifications. The development of a 3D camera technology has the potential to revolutionize the beef industry by providing real time objective measurements to assist producers improve management decisions. The new 3D technology will also provide the beef industry with a method of collecting large quantities of data to assist in making breeding decisions.

How it was done
Working in collaboration with the University of Technology Sydney we have developed software that creates a feature vector from 3D images to assess hip height, P8 fat and muscle score on live cattle within 15 seconds. A machine learning technique is employed on a ground truth dataset of ultrasound P8 fat (mm) and assessed muscle score by a trained assessor. Additional feature vectors were evaluated along with a Convolution Neural Networking technique to improve the assessment of P8 fat.

What was achieved?

- A light weight auto-calibration apparatus called the “GUBE” was developed.
- Detection of stability of 3D image generally found within 1 minute.
- Demonstration that software has been extensively developed to perform the feature extraction and assessment of P8 fat and muscle score from machine learning.
- Improved the assessment of P8 fat through:
    - Exploring alternative feature vectors
    - Exploring Convolution Neural Networks
- Developed a prototype measurement chute
- Conducted two trials on cattle that had not been seen by the cameras.

Industry benefits – results and implications

- 70% of assessed P8 fat using the 3D camera technology lies within an accuracy of ± 1.5mm
- 97% repeatability (n = 30) across 4 sessions for assessment of P8 fat within ± 1.5mm
- 77% of assessed muscle score using the 3D camera technology lies within an accuracy of ± 1 on a 15 point scale
- 80% repeatability (n = 30) across 4 sessions for assessment of muscle score within ± 1 on a 15 point scale
- 3D technology reduces variability of subjective measurements
- One off cost for 3D technology – quick return for investment
- Objective measurements on live cattle to revolutionize the beef industry

Table of contents

1 Background

This project builds upon research carried out in the 'proof of concept' (B.BSC. 0339) study supported by MLA concerning trait assessment using RGBD camera technology. Specifically, this project extends the research already conducted using 3D images for assessing live animal P8 fat (mm) and muscle score in the NSW DPI Glen Innes low and high muscling Angus herd.

The proof of concept research undertaken (B.BSC. 0339) uses commercial off the shelf RGBD cameras to capture 3D images of live cattle. A novel representation of 3D bodies related gross body shape, through curvatures, to phenotypic traits via a supervised learning framework. The 'proof of concept' studies investigated and reported the optimal sensor placement and sensor coverage strategies that would yield the highest possible accuracy in estimating the traits. Details of the 3D imaging trait estimation approach are reported in Australian Provisional Patent Application No. 2014903163 filed by MLA, NSW DPI and UTS on 3rd September 2014.

This research addresses the value proposition for the beef industry that "On-farm RGBD cameras will assist the beef industry move towards a value based trading system".

This project was specifically aimed at developing a portable on-farm 3D imaging technology for Angus steers/heifers for use at feedlot entry. A study on farm at Burmah Paraway Pastoral Co and a study at the University of New England (UNE) Tullimba feedlot were also conducted to evaluate the on-farm system using 3D cameras.

2 Project objectives

The technology developed in this project combines 3D capture, measurement of height, weight and RFID tag in a portable chute and generates outputs of hip height, muscle score and P8 fat in real time.

The project objectives were:

- Determine configuration of cameras and simple calibration procedures
- Animal stance design to allow developing adequate 3D model capture and practicality for deployment in field. This includes animals standing on a weighing platform.
- Develop the data framework for in-situ extraction 3D body representation related to gross body shape, through curvatures
- Develop the supporting machine learning framework to produce trait estimates
- Design, plan and construct a prototype chute.
- Conduct two trials at feedlots using the 3D camera system to assess in situ muscle score, hip height and P8 fat

3 Methodology

3.1 Determine configuration of cameras and simple calibration procedures

Auto-calibration is an important step in developing a robust 3D camera system. The final end point is an Airbox (a final view of alignment) that contains the image that is used to assess P8 fat (mm) and muscle score. This section provides detail on how the development of an auto-calibration apparatus has evolved by:

1. Stepping through the development,
2. Illustrating a view of an Airbox of the auto-calibration apparatus, and
3. Graphically comparing the images of an animal using 2 auto-calibration apparatuses.

A demonstration of how the original auto-calibration apparatus the “XmasTree” (Fig. 1) created a final alignment is illustrated in Fig. 2. The Xmas Tree proved to have several deficiencies:

1. Where the Xmas Tree apparatus required a manual alignment on Frames when fine tuning of the Frame was required, and
2. In some instances the Xmas tree tool itself was partially visible in the frame and an Iterative Closest Point (ICP) could not find enough features to fit the initial alignment.

Therefore, the Xmas Tree apparatus (Fig. 1) has been upgraded to a light weight prototype apparatus called the “GUBE” shown in Fig. 3. The creation of the GUBE prototype is a new method of calibrating the two camera systems which is much more robust and efficient compared to the Xmas Tree apparatus. The GUBE calibration algorithm has simplified the calibration code which can be run in real time during site trails and has been a major improvement in the development of a robust 3D camera system to assess P8 fat and muscle score.

Fig. 1. The “Xmas Tree”

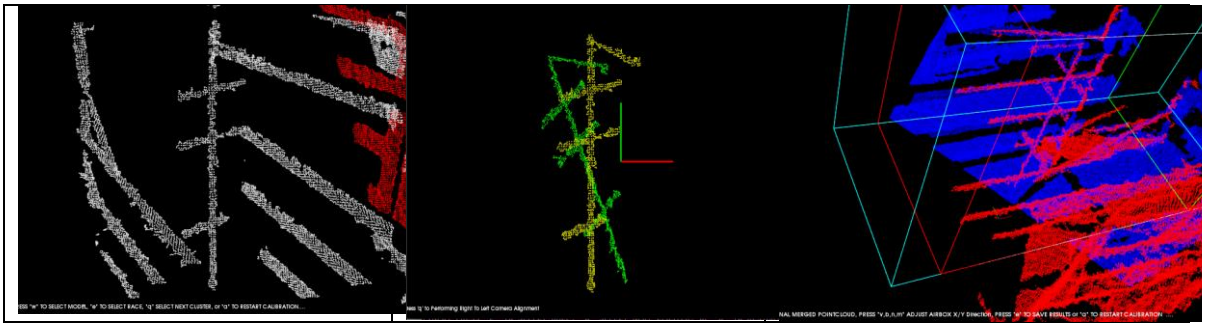

Fig. 2. Race and Xmas Tree Cluster Selection (left), Iterative Closest Point (ICP) Matching of Tree Object (centre), Final Alignment created through Xmas Tree (right)

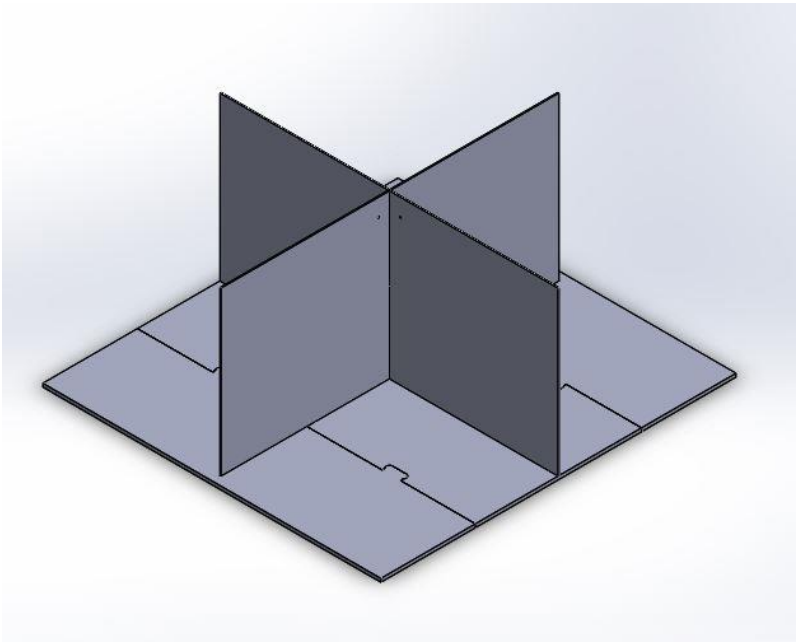

Fig. 3. Light weight prototype apparatus called the “GUBE”

The design considerations for the GUBE included:

- Three perpendicular planes which can be seen by both cameras,
- Must easily be viewed within the dimensions of cattle races , and
- Must be portable and easy for both setup and dismantling.

An important aspect of auto-calibration is alignment of the GUBE (Fig. 3). This has been achieved by implementing a Singular value Decomposition/Least Squares fit of Plane to Plane matching, where a final Iterative Closest Point (ICP) would be applied to the alignment to achieve the tightest fit. A requirement of optimising the alignment is that the cameras see some of the plane on the opposite side as seen in Fig. 4b. The Centre Axis is considered to be the x=0, y=0 location of the global coordinate frame. The height of the GUBE to the ground is also added as a constant value during calibration, to position the z=0 coordinate frame. During real time auto-calibration, the location of

the parallel parts of the lower bars of the cattle race (Fig. 4), to calculate the edges of the Airbox are also taken into consideration.

(a) (b)

Fig. 4. The GUBE is placed in line of sight to both cameras (a) and (b).

Figures 5 and 6 demonstrate the auto-calibration steps that take place in developing the Airbox (Fig. 7). A view of the final Airbox and alignment in real time is illustrated in Fig.8.

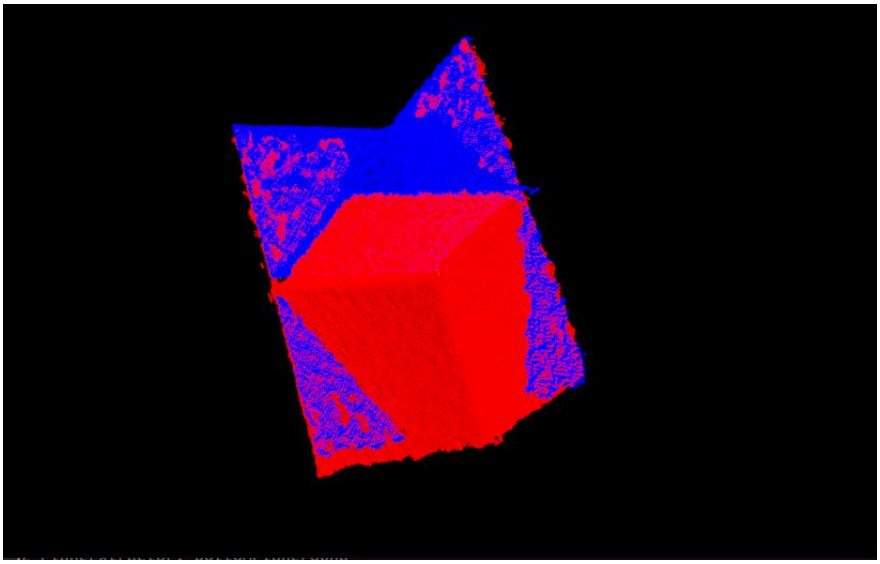

Fig. 5. Initial plane matching and alignment of the 2 cameras that can be updated in real time; Blue: Left Camera, Red: Right Camera

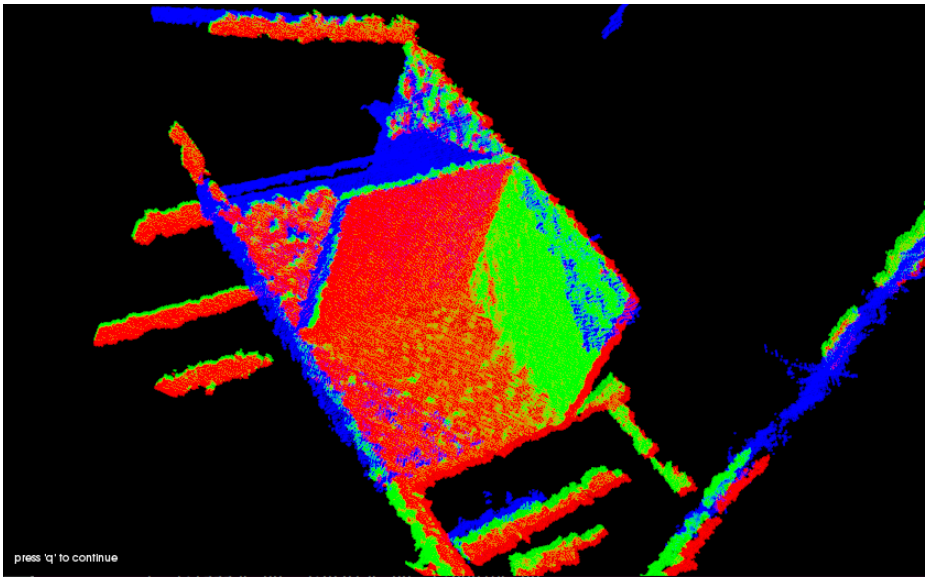

Fig. 6. Final ICP (Iterative Closest Point) alignment of the 2 cameras; Blue: Left Camera, Red: Right Camera, Green: Right Camera updated with ICP alignment

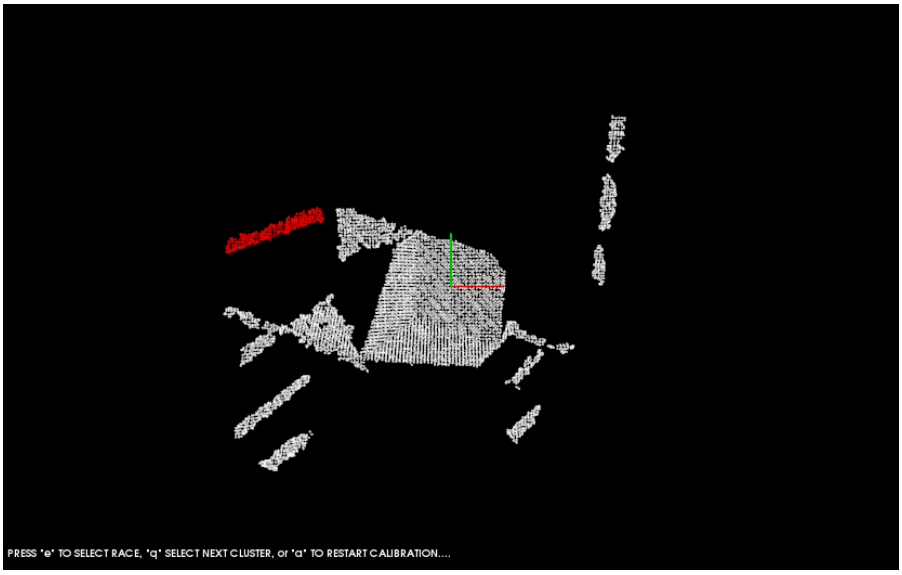

Fig. 7. Race Detection and Selection, to correctly position the Airbox

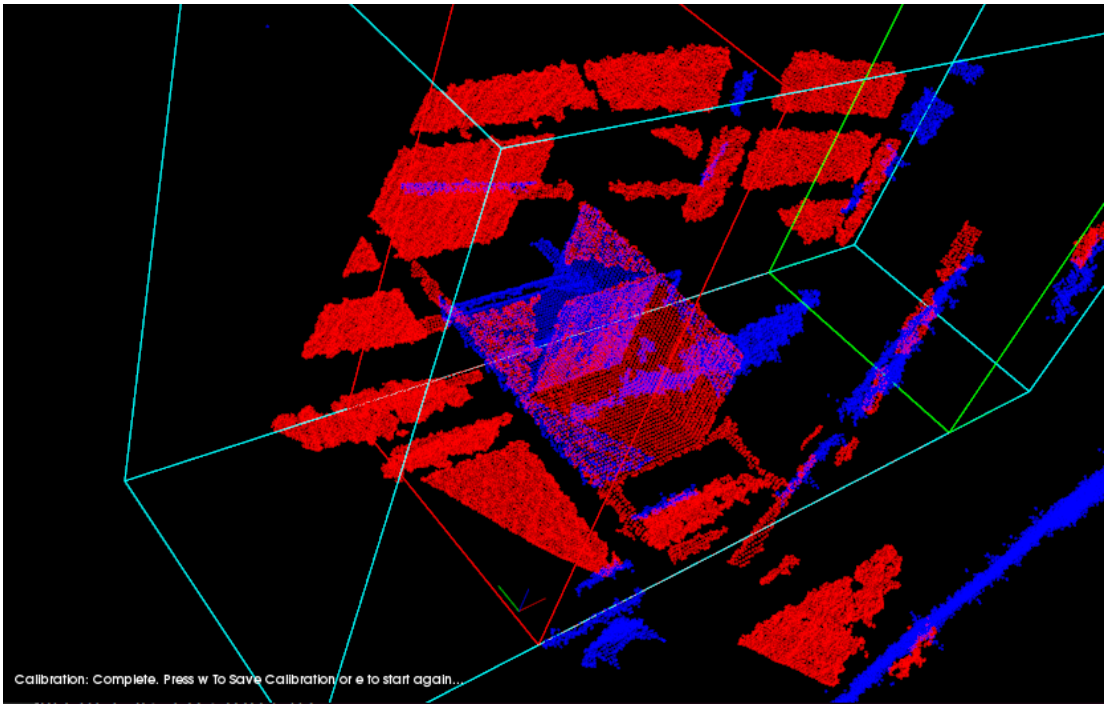

Fig 8. View of the final Airbox and alignment in real time.

Figure 9 illustrates the significant improvement (both detail and clearer image) that has been made using the GUBE as the auto-calibration apparatus as opposed to the Xmas Tree.

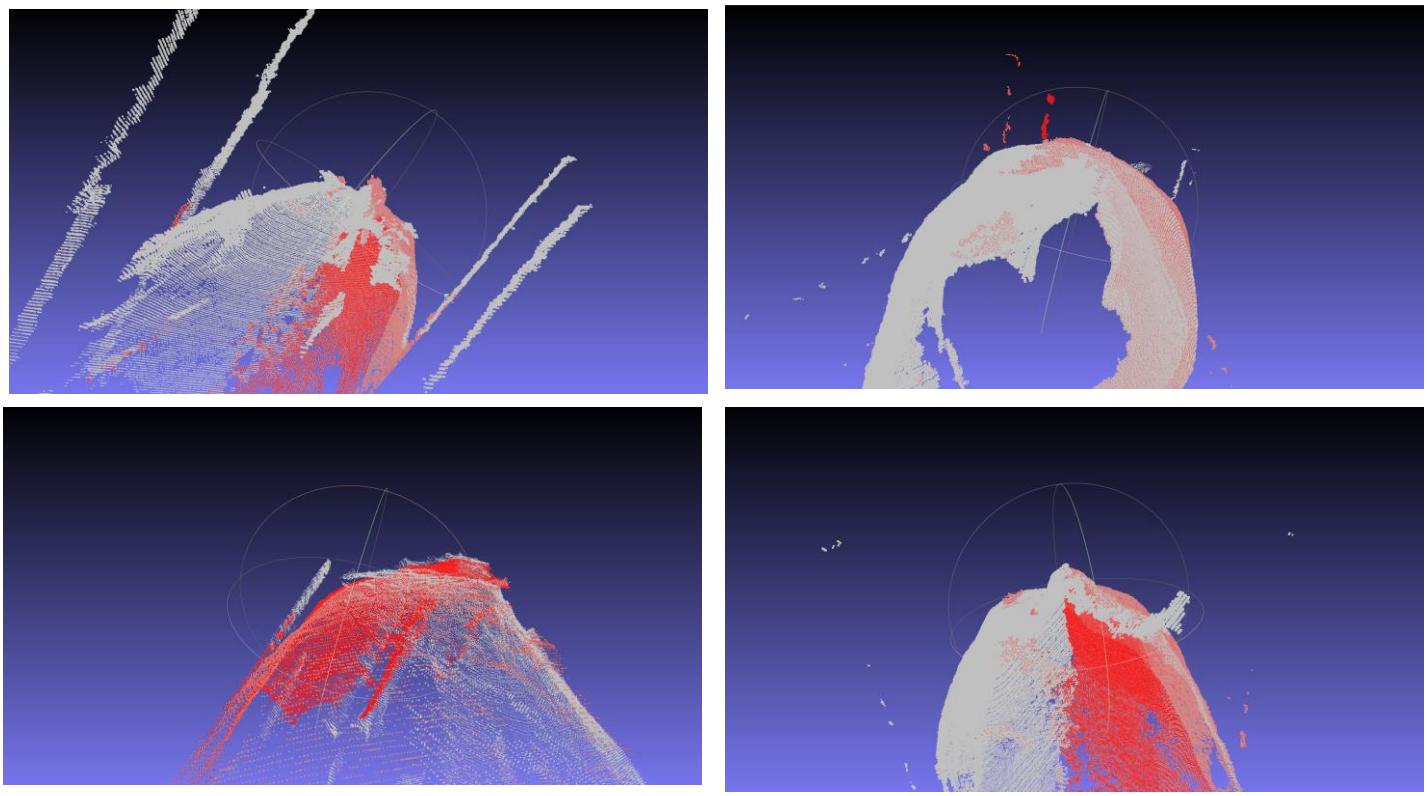

(a) Xmas Tree (b) GUBE

Fig. 9. Comparison between final alignment using auto- calibration apparatus: (a) Xmas Tree and (b) GUBE

Further research is still required to find a way to detect the change in camera position due to the animal/human disturbing the configuration. Some ideas have been investigated, including detecting movement of rails inside the race using markers in the IR (Infra Red) image. Infra Red images can also be obtained from camera and are a by-product of the depth estimation process. Research scientists are also investigating template matching in the red, green, and blue (RGB) images.

3.2 Animal stance design to allow developing adequate 3D model capture and practicality for deployment in field. This includes animals standing on a weighing platform.

Given the animals are in constant motion, even when in the chute, the approach of detecting appropriate animal stance needs to be performed at full frame rate (30fps) to allow leveraging every single frame captured from the cameras as potential 3D images for estimation.

To achieve this task, the system first detects stability (to ensure animal has reached a quasi-stationary state of motion) and thereafter is designed to transform the 3D image acquired into a consistent view for processing. Each of these processes is described in turn.

3.2.1 Stability detection and segmentation

To produce consistency in predicting a given animal, the algorithm must first be able to detect when the animal is at its most stable pose and also segment it from the rest of the scene.

Firstly, depth images are first transformed into point clouds and fused using the auto-calibration derived camera calibration parameters. This is then cropped and voxelized to only the points inside the race.

To detect stability the process involves:

- Binning the point cloud into a fixed number of segments horizontally along the animal.
- Detecting the rear of animal based on the difference in number of points between adjacent bins
- Computing height of rear (which is used in frame score calculation) and centroid value of the rear point cloud
- Computing Euclidean distance change of centroid value between frames through a sliding window approach given a time span
- Evaluating standard deviation of centroid as a proxy to determine stability

The final step is Segmentation, which is a time consuming process and batch multiple instances are completed via multiple threads to handle the load. Segmentation must be done on the original un-voxelized point cloud, with race included. The difficulty is due to the animal being in contact with the race in many cases. We cannot simply do a geometrical crop since the animal is deformable and can squeeze its self easily through the bars. To try to isolate just the animal, we use a combination of region growing on the point cloud normals, normal direction filtering, and point clustering to try and achieve consistent segmentation. In 90% of cases we have seen this method works well, there can still be some outlier cases which we still cannot handle, usually due to threshold bounds. Failures are still being investigated to be systematically removed on the processing side rather than estimation side.

3.2.2 Point cloud reorientation through spine localisation

After the best frames are detected and chosen, i.e., the frames in which the animal is in the most neutral stance observed, further processing steps are applied to ensure higher consistency between each animal instance. Greater consistency in the orientation and pose of the consolidated point clouds increases the discriminative power of the selected feature vector, since relevant regions captured by the feature vector are compared to the same regions on each animal.

The initial proposed approach of “symmetry descriptors” via 3D shape matching as reported by Kazhdan *et al.* (2004) was computationally intractable for real-time operation. Therefore an alternative exploiting the knowledge of the rough appearance primitive (quarter of a sphere / cylinder) was exploited.

Since animals vary in size, one method for consistently aligning the consolidated point clouds is to detect the spine of the animal and use this feature to re-orient and center each animal instance. The spine is detected by slicing the original point cloud along the x-axis (already undertaken for stability

detection). For each slice, the tallest point of the animal is recorded. A line is fitted through the set of tallest points. This 2D line, ignoring the z-axis or height of the animal, is considered to describe the animal's orientation, and the consolidated point cloud can be rotated and translated such that the spine is in line with the x-axis. Data is often missing along the spine region of the animal due to acuate angles between the IR light emitted from the camera and the surface orientation. As a result of this missing data, the point with the highest z value, for a given slice along the x-axis, may not accurately indicate the spine of the animal. Missing data can be interpolated, and this reduces the error in spine position but does not eliminate it, and can result in misaligned animals (Fig. 10).

Alignment and centering of the animal along its spine does not resolve ambiguity in the x-axis, e.g., one animal might be standing further along the x-axis, further along in the race, compared to another animal. Currently, alignment along the x-axis is based on finding the point with the minimum x value. However, the highly mobile nature of the animal's tail means there is often great variation in the position of this point. Future work aims to identify and remove the tail from the consolidated point cloud, or use other anatomical features to align animals along the x-axis, such as detecting the rump, pin bones or the area around the hips.

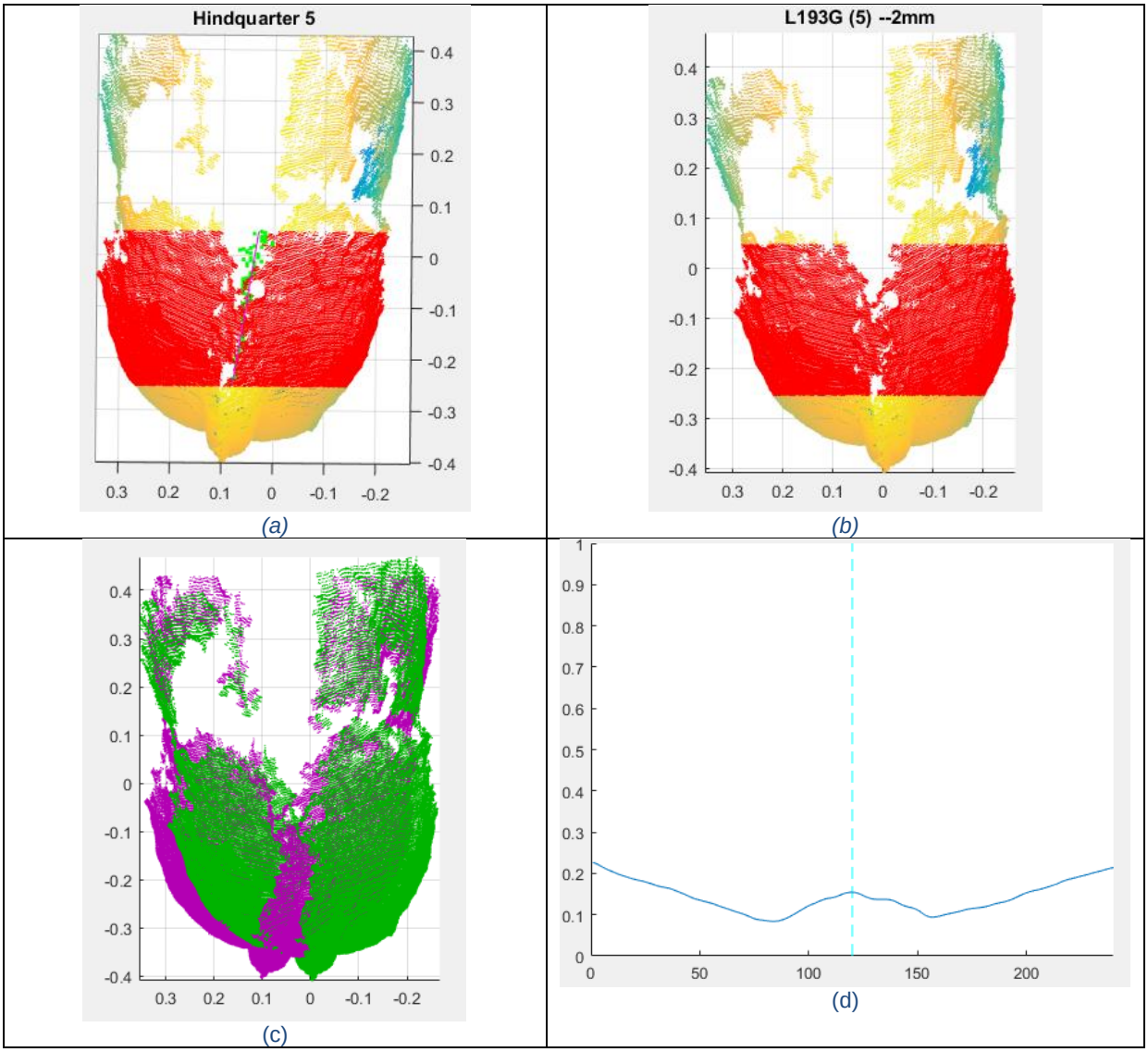

Fig. 10. The reorientation process, (a) consolidated point cloud of an animal hindquarter (red points show the region of interest, green points show the interpolated spine points, and the magenta line shows the estimated spin orientation. (b) The corrected hindquarter, and in red, the new region of

interest. (c) overlay of the hindquarter before correction (magenta) and after rotation (green). (d) example distance-from-centroid function for a single slice of an animal's hindquarter.

3.3 Develop the data framework for in-situ extraction 3D body representation related to gross body shape, through curvatures

The software processing system was divided into front-end and back-end, where front-end parts of system were required to operate at frame rate (30fps) and back-end parts required more CPU and can be done in batches.

Therefore, *front-end processing* stiches images and looks at motion while *back-end processing* performs the feature extraction and estimation from machine learning. In order to devise this software processing system a number of decisions with respect to software and processing framework have been undertaken that have translated into the implementation. The justifications for the system design follow below in section 3.3.2.

3.3.1 PC Hardware selection

Due to stateful algorithms (the output of the algorithm depends on intermediate steps, these are procedural, and cannot be implemented in parallel). For example, the Radius Outlier Removal (ROR) filter relies on all neighbouring points, a removal of one point affects the neighbourhood points (state of entire system of points), thus cannot be done in parallel. Therefore, a multicore option instead of multithreaded (GPU or CPU) option has been perused. We have converged on Intel 10-core option with multi USB bus support.

3.3.2 System Design

Design messages for System Back-Front end communication

The front and back end are still not in complete two-way communication, this is currently undertaken by a GUI that the operator uses until complete autonomy of system is desired.

Wrapping MATLAB within a Nodelet

MATLAB GMPL (http://ww w.gaussianprocess.org/gpml/code/matlab/doc/) is still used for machine learning support. The amount of information sent to MATLAB has been reduced therefore no specific nodelet is required. Implementing a service call in ROS (Robotic Operating System Middleware) directly to Matlab is an option that will be pursued. Initialising the Matlab or ROS-Matlab script would need to acquire all initialisation data from a common XML file.

Support for the machine learning frameworks in pure C++ code is minimal. At this stage MATLAB will continue to be used and will be embedded in the framework and included as a start-up service.

Wrapping Point cloud Library (PLC) code into framework

Initially the code to extract features was not integrated into entire estimation framework, after the bare bones system was implemented (Section 3.5), wrapping the PLC code with YAML was undertaken and integrated into system.

3.3.3 Efficiency testing of curvatures

The results of using surface curvatures that have been selected for the current proto-type is combined with the analysis and is reported in section 3.5.

Apart from using the surface curvature features reported in B.BSC. 0339, a number of other curvature representations have been explored in order to improve robustness of the system and generalisation (application of estimation to a wider range of Angus cattle).

Alternative Feature Vectors: Bending Energy and Hjorth Activity of Surface

Several new feature vectors have been constructed and used in machine learning models to test their ability to discriminate between fatter or thinner animals, i.e., animals with different levels of P8 fat. Intuitively, fatter animals are more rounded compared to animals with less fat. More concretely, the curvature of an animal is affected by the presence of subcutaneous fat. Capturing information about surface curvature is therefore expected to capture information about fat depths.

Curvature information is captured from consolidated 3D point clouds in using the following approach. The point cloud is first rotated and translated such that the poses and orientations of each animal's point cloud are as consistent as possible. A central line is defined at a fixed distance below the highest point of the animal, running along the x-axis, i.e. along the now aligned spine of the animal. The point cloud is then divided into slices, starting from the rear of the animal and moving towards the front. The central line defines a single point per slice, called the centroid, from which a ray can be cast outwards, at a desired angle, with an angle of 0 degrees resulting in the ray pointing in the negative z direction, and an angle of 180 degrees resulting in the ray casting outwards from the centroid up in the positive z-direction and intersecting with the spine of the animal. An angle from 0 to 360 results in a ray that passes within some distance of the points in that slice of the point cloud of the animal. The subset of points within a maximum distance of the ray can be determined, and averaged into a single value, describing the distance along a ray at that angle from the centroid of the slice to the mean of the points sufficiently close to the ray.

A function is therefore created which relates angles from 0 to 360, to the distance of the outer surface of the animal to the centroid. A function (Fig. 11) is generated for each slice.

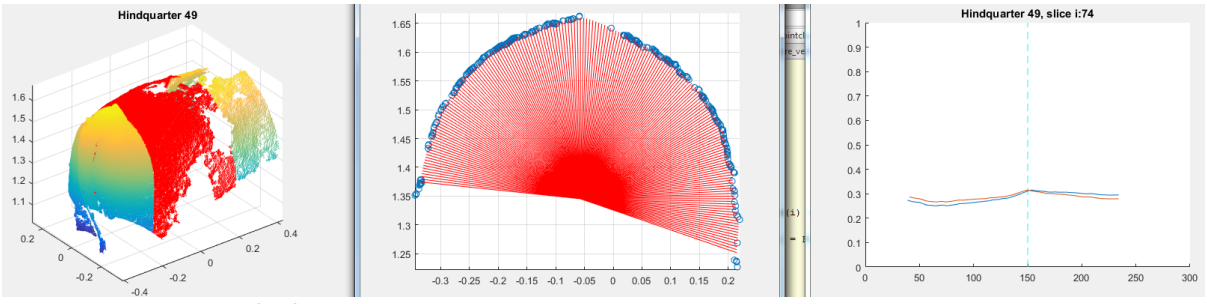

Fig. 11. Generation of a function which relates to angles 0 to 360.

Two feature vectors are created from this distance function. The first is Bending Energy, which is defined as the averaged sum of the second derivative of the function described above. A single Bending Energy value is calculated per slice, and the vector of these values is the feature vector.

The second feature vector calculates the Hjorth activity value of the distance function, and also results in a single value per slice, which becomes a vector of values.

The angles defining the domain of the function are restricted to values that are reasonably, i.e. likely to have consistent data across each animal. The number of slices is restricted to a fixed number, defining a fixed distance from the starting x-value, at a chosen offset from the point with the minimum x-value.

On individual animals, the functions seem reasonable. The animal is rounder towards the hip compared to the pin bones, and this is reflected in the higher bending energy values around the pin-bone versus the bending energy values around the hip.

Unfortunately, when these feature vectors were used in a GP to predict the fat depth of different animals, no statistically significant estimate of P8 fat depth was possible.

There are several underlying issues that contribute to the fragility of these two feature vectors. The first is the alignment of each animal. Alignment along the spine is successful for some animals, but not others, and some residual error remains. Alignment along the x-axis, in particular the effect of the tail, has not been sufficiently addressed. A final issue is one of scale, whereby the distance from one animal's pin bone to the hip is different to another animal; and yet comparing these same regions is important. At present, no scaling takes place. The result of misalignment is that elements of the feature vector of one animal do not correspond to the same element of another animal's feature vector, i.e. the elements relate to different regions of the animals' surfaces.

Future work will endeavour to resolve these alignment issues, which are fundamental in ensuring the robustness of any feature vector based on geometric information such as is available in the consolidated point clouds in the current data set.

3.3.4 System testing of optimal learning framework

The optimal learning framework has evaluated several frameworks for regression and classification (GPML, MatSVM, LibSVm, NN, and MatGP) (McPhee *et al.* 2017).

In order to boost generalisation, an approach to use Deep Learning (Convolution Neural Networks) was investigated. The ConvNet / CNN's are a category of convolution neural networks that have proven to be very effective in the areas of image recognition and classification Krizhevsky *et al.* (2012). This change in research direction builds upon our previous research effort in the area of biological trait estimation (prediction) for cattle using state-of-the-art machine learning techniques and 3D point cloud data.

Our earlier research efforts relied upon careful selection and creation of a specific feature vector, which was thoughtfully derived from the original 3D point cloud data collected in the field. This feature selection (creation) step is common practice in traditional machine learning. It is important to accept that crafting a descriptive feature vector that is representative of the underlying data is tantamount to the success of the overall machine learning process.

However, Convolutional Neural Networks (ConvNets or CNN) are widely used methods for Deep Learning that does not require construction of a feature vector prior to training or testing. Using the appropriate convolutional neural network architecture allows important features to be determined automatically and stored within the CNN model during training and testing phases of learning (Bishop 2006; Murphy 2012).

Convolutional neural networks are inspired from the biological structure of a visual cortex, which contains arrangements of simple and complex cells (Hubel and Wiesel 1959). These cells are found to activate based on the sub regions of a visual field. These sub regions are called receptive fields. Inspired from the findings of this study, the neurons in a convolutional layer connect to the sub regions of the layers before that layer instead of being *fully-connected* as in other types of neural networks. The neurons are unresponsive to the areas outside of these sub regions in the image. These sub regions might overlap, hence the neurons of a ConvNet produce spatially-correlated outcomes, whereas in other types of neural networks, the neurons do not share any connections and produce independent outcomes.

Additionally, convolutional neural networks reduce the number of model parameters with the reduced number of neuronal connections, shared weights and down sampling layers (max or mean pooling). The convolution neural networks employed in this research typically consist of multiple layers (Krizhevsky *et al.* 2012) as in Fig. 12.

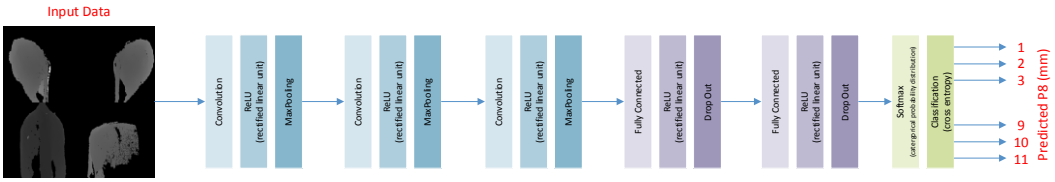

Fig. 12. Typical Convolutional Neural Networks Architecture used for Deep learning in this study.

Convolutional neural networks are specifically suitable for 2D images as inputs, although they are also used for other applications such as text, signals, and other continuous responses (LeCun *et al.* 1998; Nair and Hinton 2010; Nagi *et al.* 2011; Srivastave *et al.* 2014). As such, we extract the LEFT and RIGHT 2D depth images for each data frame captured in the field using the 3D RGBD cameras. Additionally, the corresponding REAR and SIDE images were also computed using ray tracing methods, which provided a total of four different image perspectives of each frame of data as illustrated in Fig. 13.

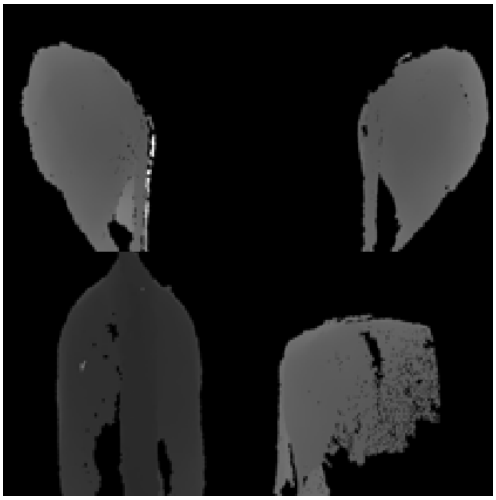

Fig. 13. A single Quadrature Depth Image (224x224x1) used as input to the Convolutional Neural Networks. The Quadrature depth image consists of LEFT, RIGHT, REAR and SIDE perspectives of for every single frame of an individual animal.

We computed a set of 2D quadrature depth images from recently acquired 3D RGBD data from Tullimba_2016_10 (Tullimba 2016) and Inverell_2017_04 (Inverell). To increase the classification performance (accuracy) of CNN in a deep learning setting, large amounts of input data is required during training. As such, we developed data augmentation algorithms to increase the number of 2D quadrature depth images and provide an even number of images across the target P8 ranges from 2mm-11mm.

Data augmentation was applied to the LEFT, RIGHT, REAR and SIDE images individually. Transformations were applied randomly within predefined bounds and included rotation, translation, shearing, noise (holes), noise (entire image) and noise (per pixel) as illustrated in Fig 14.

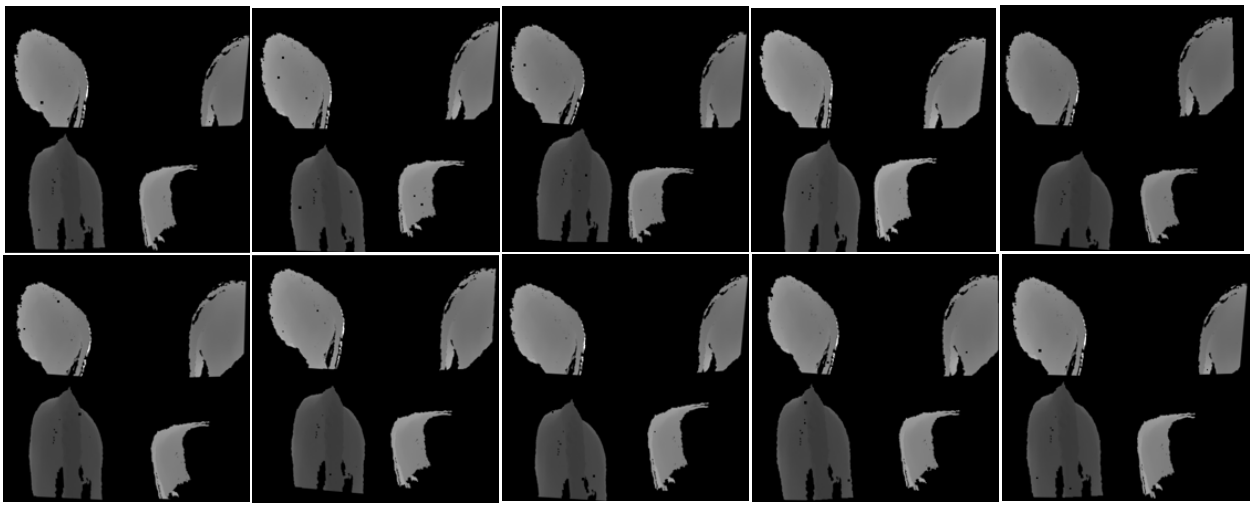

Fig. 14. Ten augmented quadrature depth images of a single frame for an individual animal.

In total, approximately 188,000 2D quadrature depth images were used for training and 8000 images for testing the CNN performance.

Due to the intrinsic error associated with the P8 ground truth data (±1.0mm), the P8 classes were combined into the following arrangements: Class 1 = {2, 3, and 4} mm, Class 2 = {5, 6, and 7} mm and Class 3 = {8, 9, 10, and 11} mm.

The ConvNet training procedure generally follows Krizhevsky *et al.* (2012). Namely, the training is carried out by optimising the multinomial logistic regression objective using mini-batch gradient descent (based on back-propagation LeCun *et al.* (1998) with momentum.

In the preliminary investigation of applying CNNs on trait estimation undertaken for this project, a number of parameters of the learning framework were evaluated empirically with respect to system performance. Batch size was set to 128 images and momentum 0.9. However, the batch size was increased to 256 for CNN architectures that contained a smaller number of layers and less filters per layer. The training was regularised by weight decay (the L2 penalty multiplier set to $5x10^{-4}$) and dropout regularisation for the first two fully-connected layers (dropout ratio set to 0.6). For random weight initialisations, we sampled the weights from a normal distribution with the zero mean and $1x10^{-2}$ variance. The bias vectors were initialised with zero. The initial learning rate was set to $5x10^{-4}$ with a piecewise learning rate schedule that dropped by a factor of $1x10^{-1}$ every 10 epochs. The maximum number of epochs was set to 20 or 30 epochs, depending on the CNN architecture being investigated.

Training was performed on a single NVIDIA TESLA P100 GPU with 16GB of on board DDR5 memory and CUDA version 375.39. Preliminary results (Table A) indicate the system is capable of learning across the two datasets (Tullimba 2016 and Inverell) with a marginally lower RMSE on the animals with low P8 fat than that reported with current system using curvatures. The latest Tullimba dataset (Tullimba 2017) acquired in August 2017 at a demonstration of the real-time 3D camera technology to MLA and NSW DPI managers has also been used to evaluate the accuracy of assessment and results are reported in section 4.3. Though low P8 values are discriminated well with CNN, the medium values suffer being overestimated. 23 CovNet's of various size have been evaluated with only subtle differences being observed, those reported in Table A are indicative of system performance.

Table A. Confusion matrix (proportion of correct classifications within classes) using a 4x8 Convolutional Neural Network (ConvNet) of completely unseen data (45 images for testing results) for single data set (Inverell) and double data set (Inverell and Tullimba 2016). Rows add to 1.

Class 1=[2,3,4mm], Class 2=[5,6,7], Class 3=[8,9,10,11];

ConvNet	SINGLE DATA SET		
4x8	Class 1	Class 2	Class 3
Class 1	0.51	0.29	0.19
Class 2	0.22	0.27	0.51
Class 3	0.15	0.30	0.55

ConvNet	DOUBLE DATA SET (SD)		
4x8	Class 1	Class 2	Class 3
Class 1	0.71	0.24	0.05
Class 2	0.13	0.25	0.62
Class 3	0.11	0.27	0.62

3.3.5 Estimation Pipeline Automation

The pipeline architecture has now been completed with a series of linux scripts to simplify the pipeline during post-processing of data. The data generated within the pipeline is now structured in

a readable format and is easily manipulated. These new modifications to the pipeline provide quick implementation and control messages between different applications while still maintaining possible manual control. Simply put, the speed of post-processing of data has increased; the machine learning and prediction process is quicker. An integrated pipeline which is robust and efficient for real time conditions has been achieved.

The system currently estimates the stability in real-time, requires 40-50s for processing point clouds (feature extraction) and 4s to estimate the trait from the features using machine learning. Therefore, the animals can be fed through every minute as the system does not require animals to be present within the chute in the point cloud processing stage. However, if for some reason the point cloud data is not a good representation (for instance, the tail of animal was in contact with body, and unable to be removed), then releasing the animal would result in no estimate being produced.

3.4 Design, plan and construct a prototype chute.

Modifications to the original aluminium measurement chute (B.BSC. 0339) have been conducted. The modifications included: decreasing the length of the chute, development of bars where cameras could be positioned, stands for cameras to be positioned on, and shading.

The redesign and modification of the current chute to improve portability has been undertaken. A professional saddler was hired to develop a canvas shade covering to reduce the sunlight

3.5 Conduct two trials at feedlots using the 3D camera system to assess in situ muscle score, hip height and P8 fat

Two trials have been conducted using the 3D system to asses in situ muscle score, hip height and P8 fat. The trials were conducted at the Inverell Burmah Paraway Pastoral Co property; and the UNE Tullimba feedlot.

The portable measurement chute was set up at end of the crush at each of these locations.

4 Results

4.1 Develop the supporting machine learning framework to produce trait estimates

Experimental data for the development of machine learning algorithms to produce trait estimates of P8 fat (mm) and muscle score were conducted at the UNE Tullimba feedlot facility (Tullimba 2016) and the Pastoral Paraway Co Burmah property near Inverell (Inverell). The frequency histogram of the Tullimba 2016 and Inverell P8 fat (mm) and muscle score data are illustrated in Fig. 15 to 18.

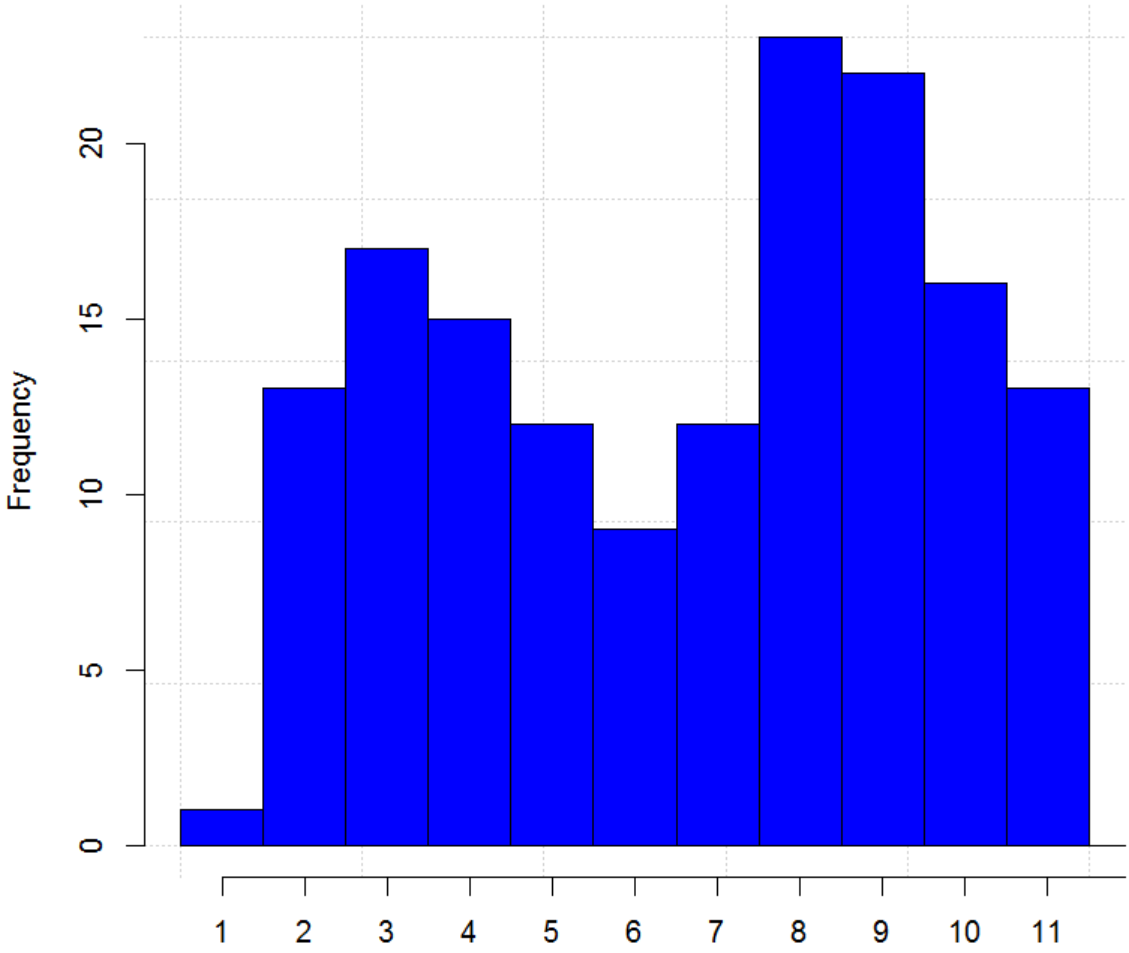

Fig. 15 Frequency histogram of the assessed ultrasound P8 fat (mm) for the Tullimba 2016 data

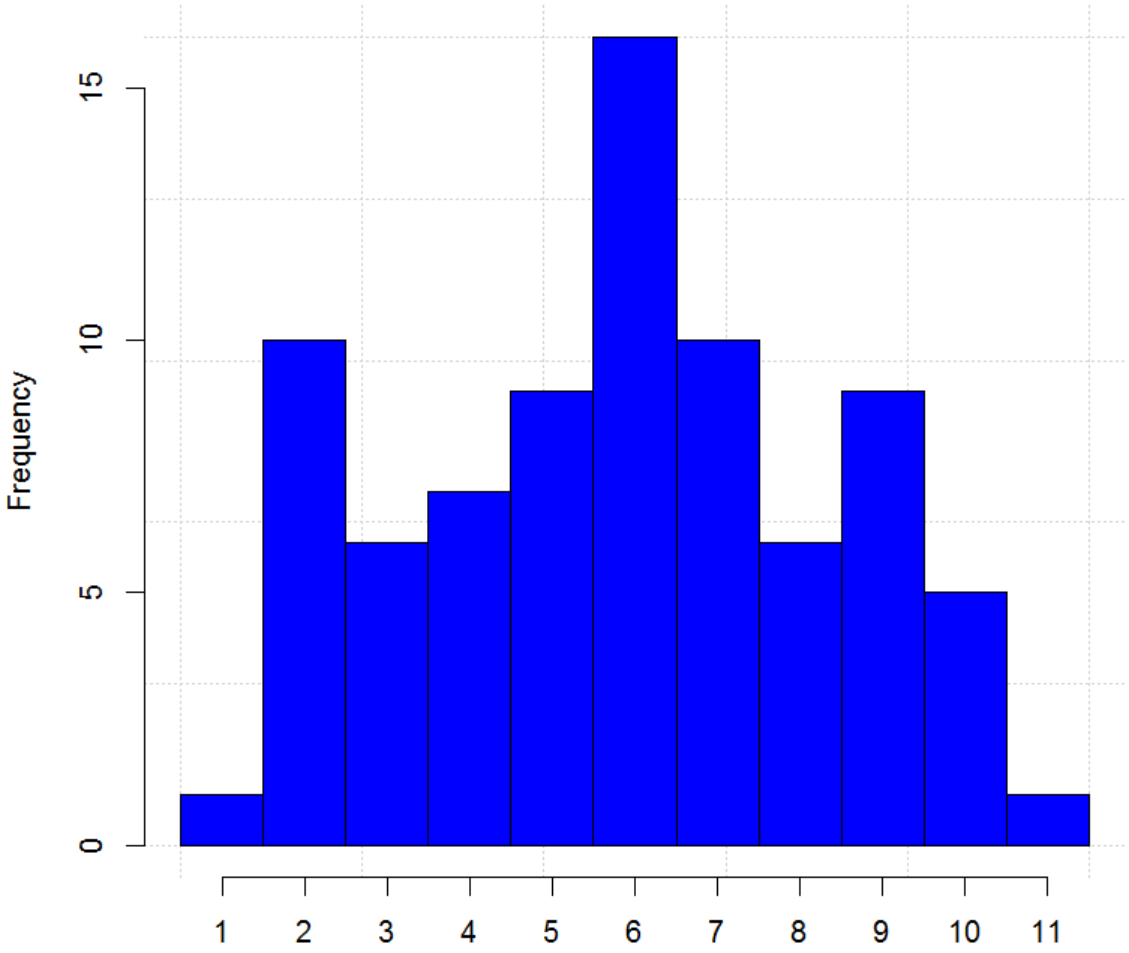

Fig. 16 Frequency histogram of the assessed ultrasound P8 fat (mm) for the Inverell data

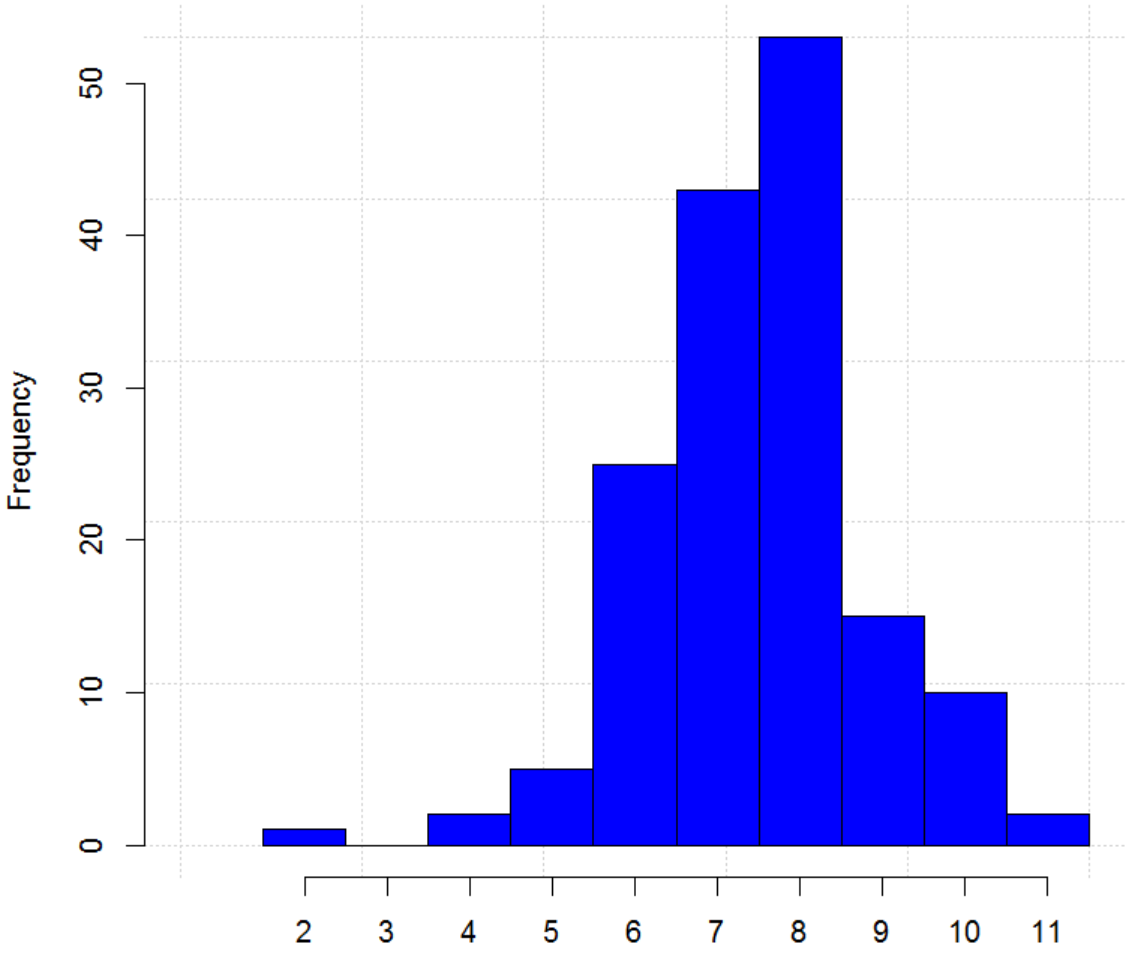

Fig. 17 Frequency histogram of the assessed muscle score on a 1 to 15 scale for the Tullimba 2016 data

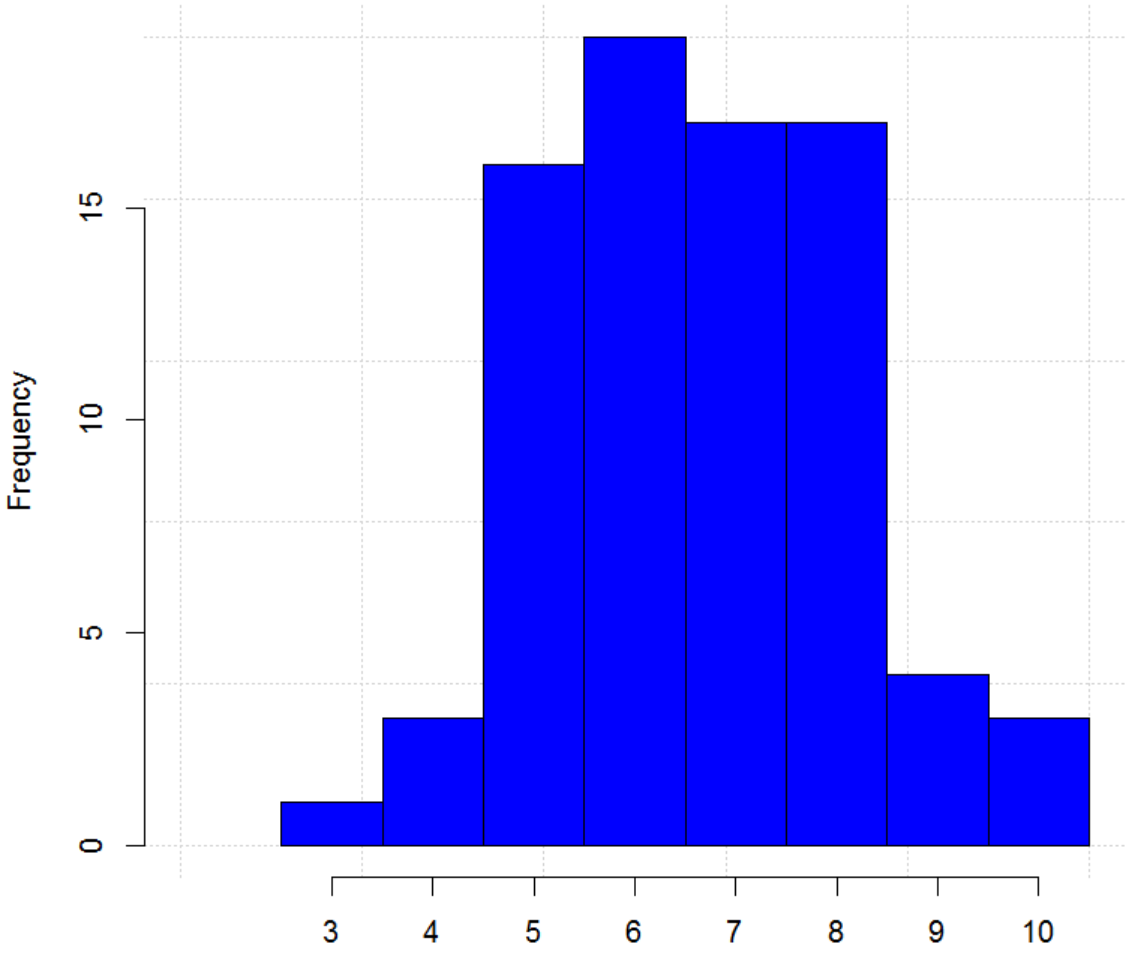

Fig. 18 Frequency histogram of the assessed muscle score1 to 15 scale for the Inverell data

The results of the 3D camera P8 fat (mm) model built on the UNE Tullimba 2016 data and 10 fold cross validated on the UNE Tullimba 2016 data are reported in Fig. 19.

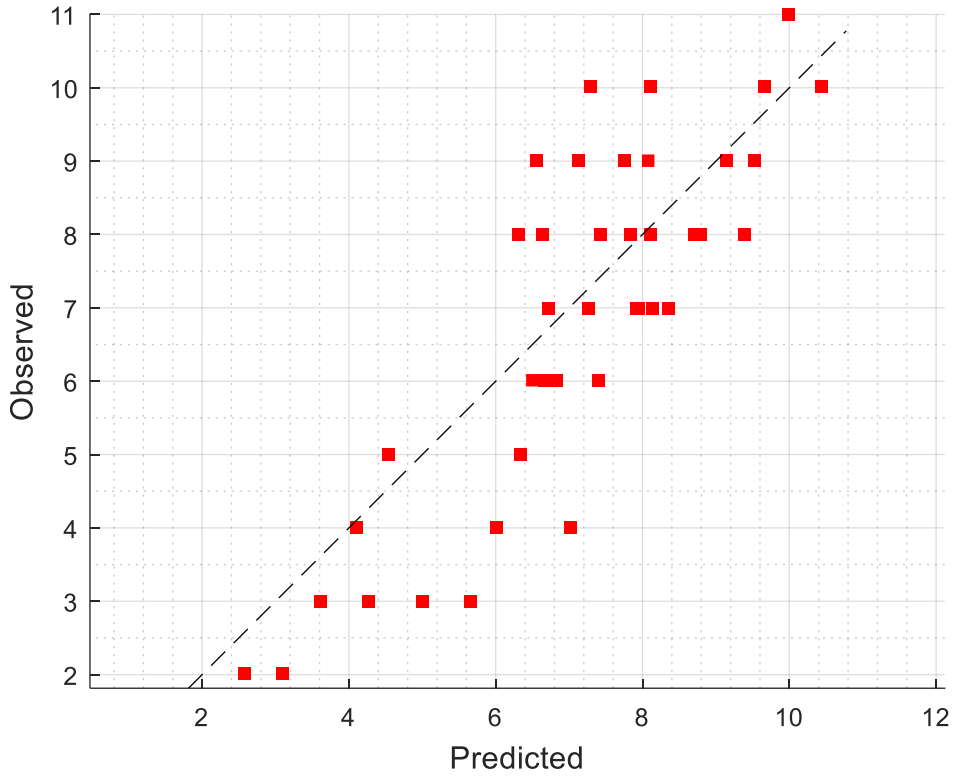

Fig. 19. Model built from Tullimba 2016 data and tested on Tullimba 2016 data (10 fold cross validation)

The RMSE of Fig. 15 was 1.27 mm.

The results of assessing the accuracy of assessing muscle score built from Tullimba 2016 data and tested on Tullimba 2016 data (10 fold cross validation) are reported in Table 1.

Table 1. Accuracy between the trained assessor and the 3D camera technology of the model built from the Tullimba 2016 data and tested on the Tullimba 2016 data (10 fold cross validation) for muscle score on a 1 (D-) to 15 (A+) scale. Values along the diagonal indicate the number of times the 3D camera technology assessed muscle sore as the same score.

	Assessed 3D camera technology					
Trained assessor	D-	D	D+	C-	C	C+
D-	0	0	0	0	0	12
D	0	0	2	8	0	0
D+	0	0	5	11	0	6
C-	0	5	78	146	93	4
C	0	55	35	135	86	75
C+	0	0	0	0	1	23

Table 1 indicates that the accuracy of assessment of the Tullimba 2016 data and tested on the Tullimba 2016 data (10 fold cross validation) on a 15 point muscle score scale is 33% and the accuracy within 1 bound on a 15 point scale is 84%. Note: accuracy within 1 bound is considered good.

The results of the 3D camera P8 fat (mm) model built on the Inverell data and 10 fold cross validated on the Inverell data are reported in Fig. 20.

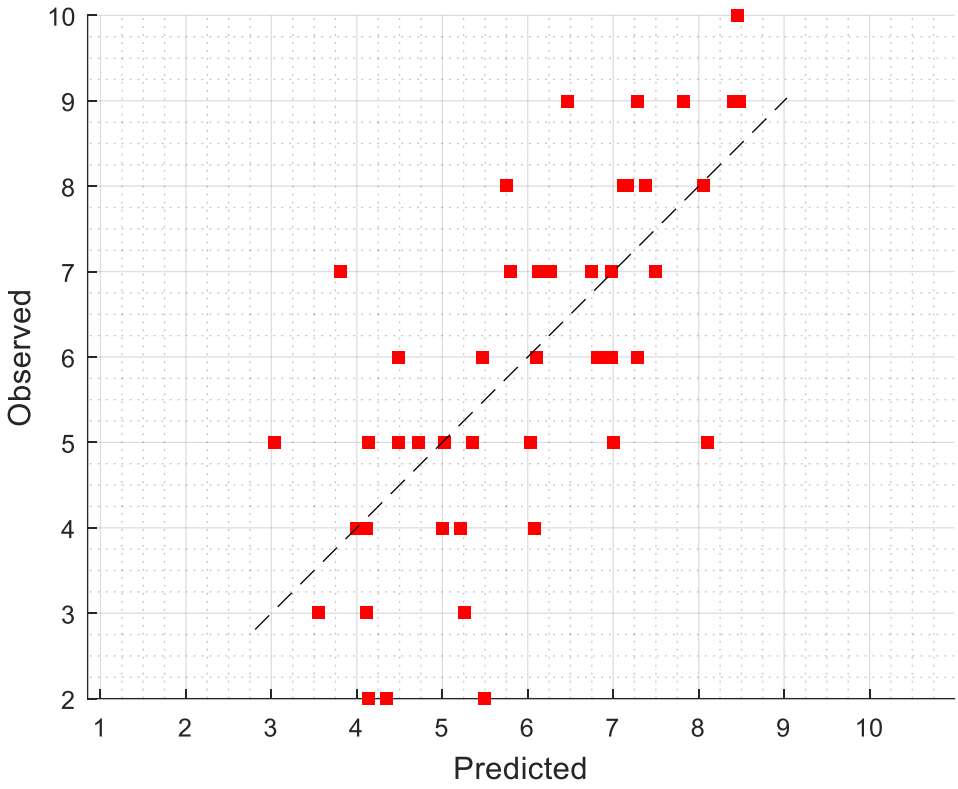

Fig. 20. Model built from Inverell data and tested on Inverell data (10 fold cross validation)

The RMSE of Fig. 16 was 1.37 mm.

Accuracy of assessment of muscle score for the model built on the Inverell data and 10 fold cross validated on the Inverell data is reported in Table 2.

Table 2. Accuracy between the trained assessor and the 3D camera technology of model built on the Inverell data and 10 fold cross validated on the Inverell data for muscle score on a 1 (D) to 5 (A) scale. Values along the diagonal indicate the number of times the 3D camera technology assessed muscle sore as the same score. Note: insufficient data for a 15 point scale.

	Assessed 3D camera technology			
Trained assessor	E	D	C	B
E	0	0	0	0
D	0	64	20	0
C	0	16	100	0
B	0	0	0	0

Table 2 indicates that the accuracy of the model built on the Inverell data and 10 fold cross validated on the Inverell data was 82%.

The results of the 3D camera P8 fat (mm) model built on the UNE Tullimba data and evaluated against the Inverell data are reported in Fig. 21.

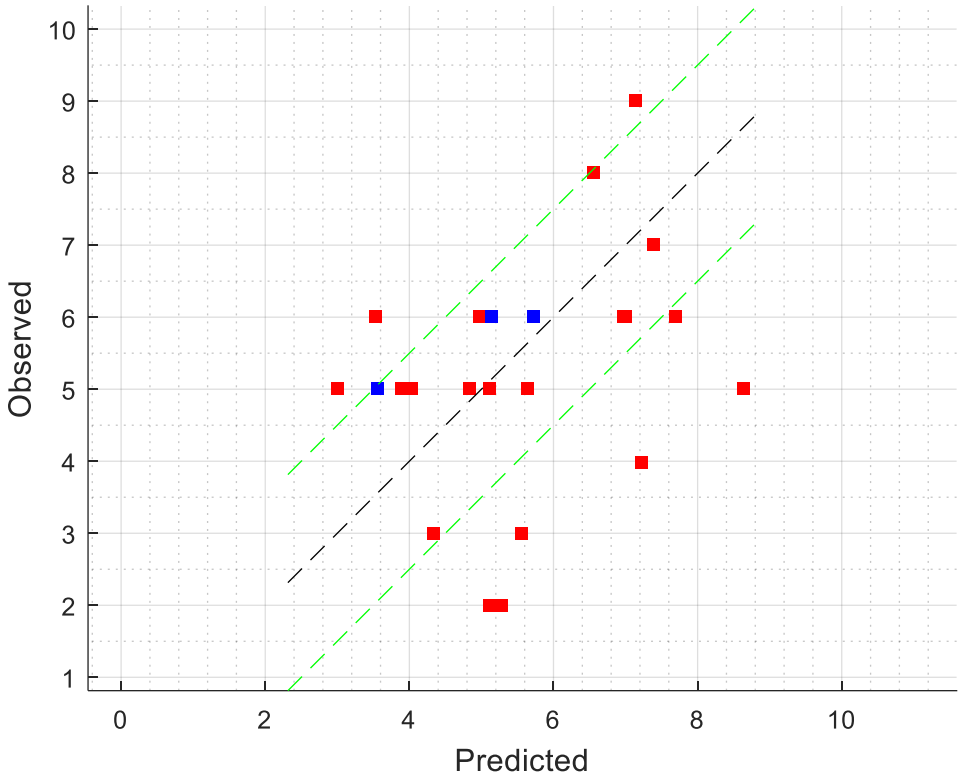

Fig. 21. Results of Inverell measured P8 fat (mm) versus estimated P8 fat (mm) based on model built on Tullimba 2016 data. Blue squares indicate uncertainty around the assessment of the 3D camera system.

The RMSE of Fig. 17 was 1.8 mm.

Accuracy of assessment of Inverell muscle score for the model built on Tullimba 2016 data is reported in Table 3.

Table 3. Accuracy between the trained assessor and the 3D camera technology built on the Tullimba 2016 data and evaluated against the Inverell data for muscle score on a 1 (D-) to 15 (A+) scale. Values along the diagonal indicate the number of times the 3D camera technology assessed muscle sore as the same score.

	Assessed 3D camera technology					
Trained assessor	D	D+	C-	C	C+	B-
D	0	0	2	0	0	0
D+	0	0	4	0	0	0
C-	0	0	12	2	5	2

C	0	0	7	1	2	1
C+	0	0	3	0	1	0
B-	0	0	1	0	0	0

Table 3. Indicates that the accuracy the 3D camera technology built on the Tullimba 2016 data and evaluated against the Inverell data on a 15 point scale was 19% and accuracy for within 1 class bound was 70%. Assessment within 1 class is considered good.

The feature vector used in our work is derived from the surface curvature, which encodes the spatial appearance of the animal, and related to the trait. In order for the curvature to be generated, a viewpoint (origin of looking at the animal) is selected. From this a point curvature is captured, in addition all points sitting on the surface of the animal also assemble part of this feature representation, contributing to a description over the convexity of the animal.

The selection of the viewpoint in object recognition (where this concept viewpoint originates) is done so that the view of the surface in its entirety can be captured. For the hindquarter region, which is relevant to the traits, and used in this analysis the point was below the animal. One could envision it as on the floor between the back legs of the animal looking up. Given the bottom surface of the animal (belly) is not captured from this vantage point an unobstructed view over the top surface (hind quarter) is visible.

This selection has distinct advantages of not having any obstructions and seeing most of the surface. However, the viewpoint also suffers from variation in height difference of the animals. Feature vectors from the two datasets (Tullimba 2016 and Inverell) in Fig. 22 and 23 demonstrate the effect of altering the viewpoint. The figures show the feature vector corresponding to a single P8 fat value (5mm) of several animals in both datasets (denoted as red and blue). The entire feature vectors should overlap, given they are the same trait. The viewpoint is altered between 5 and 6 resulting in different feature vectors. This inconsistency leads to poor estimation results.

While we have improved the estimation results altering the viewpoint in response to the data across trials, a systematic approach and one that is data driven is being investigated.

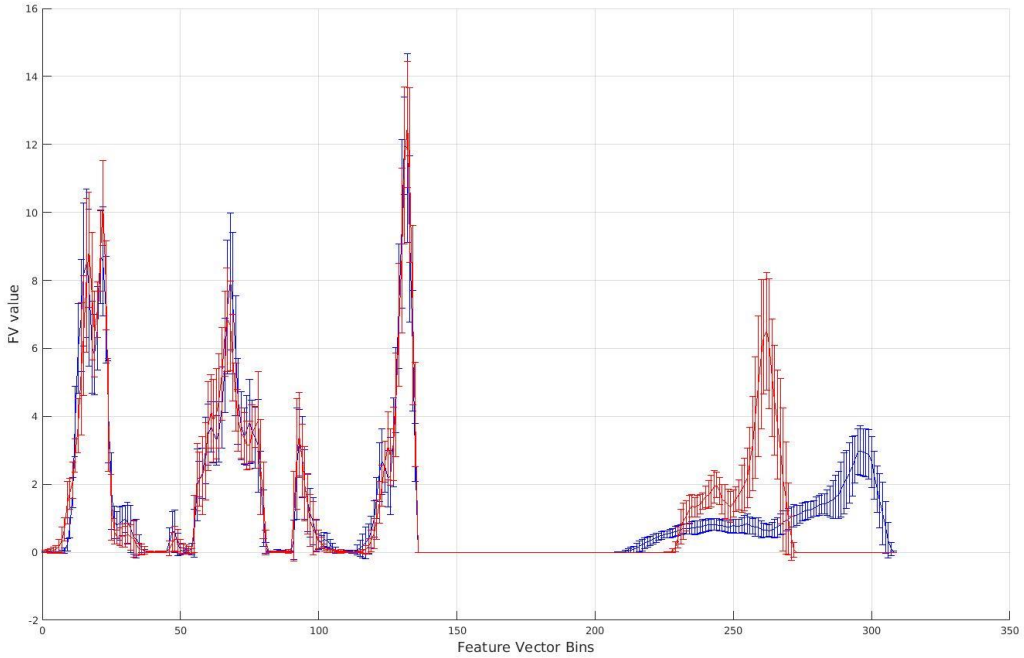

Fig. 22. Tullimba 2016 versus Inverell features (viewpoint 1)

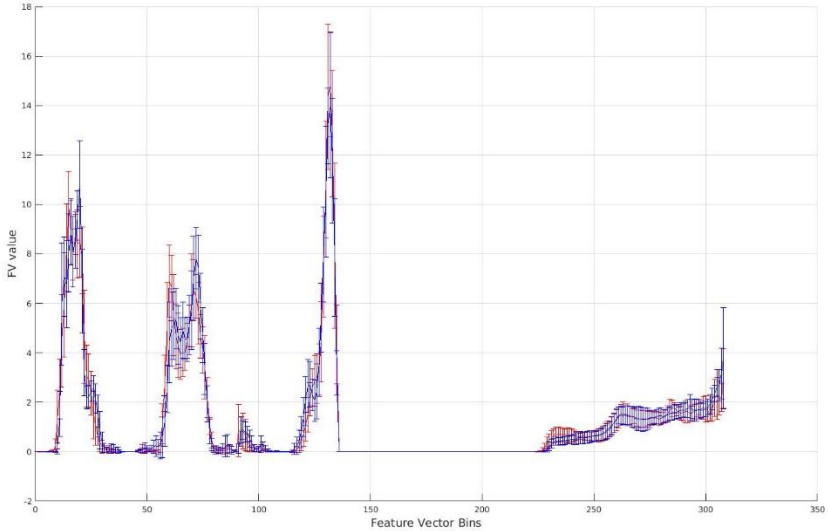

Fig. 23. - Tullimba 2016 vs Inverell features (viewpoint 2)

4.2 Design, plan and construct a prototype chute.

4.2.1 Redesign and modification of current chute to improve portability.

The portable measurement chute used at the ACC Brindley Park feedlot to collect 3D data on *Bos indicus* and *Bos indicus* crosses has been redesigned. An aluminium measurement chute used in the MLA 3D camera proof of concept project (B.BSC. 0339) has been modified to open up on the sides for the cameras to be positioned and bars to hold a canvas cover shown in Fig. 24.

Fig. 24. Opening on the measurement chute for the positioning of the cameras.

4.2.2 Modification of chute to include a method to quickly hang shade

A professional saddler was employed to develop a canvas that can be easily rolled out when bumping in the portable measurement chute as shown in Fig. 25. The canvas can be quickly unrolled when bumping in the measurement chute.

Fig. 25. Canvas shade over the measurement chute to reduce the sunlight.

4.2.3 Integration of an RFID tag reader on the measurement chute.

Integration of RFID tag read and weight scales have now been implemented into the measurement chute (Fig. 25). Figure 26 illustrates the set up as a one stop for weight, RFID reading, P8 fat and muscle score assessment.

Fig. 26. Data reporting of weight, P8 fat (mm) and muscle score

4.3 Conduct two trials at feedlots using the 3D camera system to assess in situ muscle score, hip height and P8 fat

Two trials were conducted on Angus cattle: one at the Inverell Burmah Paraway Pastoral Co property and the other at the UNE Tullimba feedlot. The Inverell dataset has been mentioned above in the development and evaluation of machine learning techniques employed in this study. The following section describes in detail a trial that was conducted at the UNE Tullimba feedlot.

4.3.1 UNE Tullimba feedlot

On-farm real-time 3D system (prototype version 2) demonstration was conducted at the Tullimba, University of New England feedlot on 29th August 2017. Twenty-seven head of Angus cattle ranging in weight were ultrasound scanned for P8 fat (mm) (Fig. 27) and assessed for muscle score on the 28th August (Table 4). Muscle scoring was based on a visual assessment of thickness and convexity of the body relative to skeletal size, with an adjustment for fatness (McKiernan, 2007). A 15-point scale was used, from E- (1), the lightest muscled, to A+ (15), the heaviest muscled (McKiernan, 2007). The 3D cameras assessed P8 fat and muscle on 4 occasions between the 28th and 29th August (Table 5) using techniques described by McPhee *et al.* (2017). Figure 28 illustrates the capturing of images that takes up to 1 min to auto detect when cattle are stable enough to take an image; after capturing the image the processing takes 15 seconds to report hip height, P8 fat and muscle score (Fig. 29).

Fig. 27. Ultrasound scanning of cattle on the Monday 28th August 2017

Fig. 28. Post processing setup for analysing images from 3D cameras

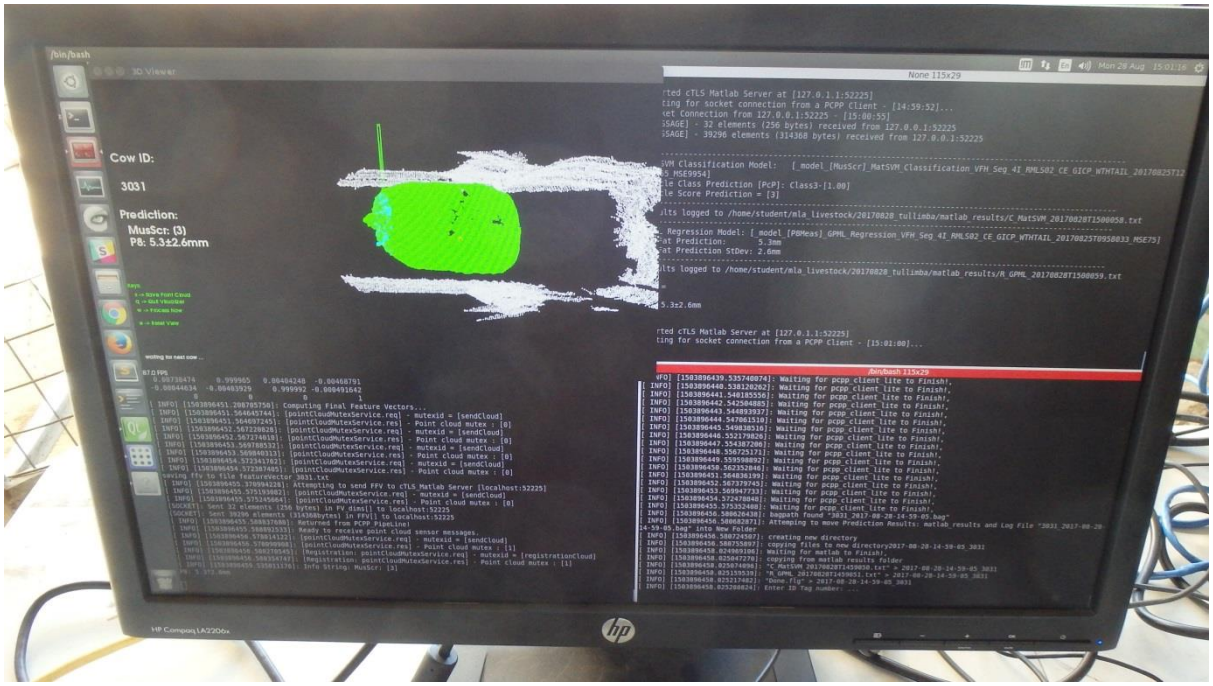

Fig. 29. On screen reporting of muscle score and P8 fat

Table 4. Summary of actual weight, ultrasound P8 fat, and assessed numerical muscle score for Angus heifers and steers

	Heifers			Steers		
	Weight (kg)	Ultrasound P8 fat (mm)	Numerical Muscle score	Weight (kg)	Ultrasound P8 fat (mm)	Numerical Muscle score
n	21	21	21	6	6	6
Min	316	2	5	348	5	7
Max	380	9	10	370	6	8
Mean	349.90	5.24	7.29	361.00	5.50	7.17
SD	17.91	2.00	1.19	8.65	0.55	0.41

Table 5. Summary of assessed 3D camera images for P8 fat and numerical muscle score for Angus heifers and steers across 4 repeated sessions

	Heifer		Steer	
	P8 fat (mm)	Numerical Muscle score	P8 fat (mm)	Numerical Muscle score
Session 1				
n	17	17	6	6
Min	3.47	6.5	3.63	6.5
Max	5.99	8.0	4.93	8.0
Mead	4.43	7.38	4.25	7.17
SD	0.74	0.70	0.57	0.68
Session 2				
n	20.00	20.00	5.00	5.00
Min	3.23	6.5	3.37	6.5
Max	5.53	8.0	4.40	8.0
Mead	4.41	7.35	3.75	7.20
SD	0.51	0.69	0.41	0.76
Session 3				
n	20.00	20.00	6.00	6.00
Min	3.62	6.5	4.02	7.0
Max	5.49	8.0	4.68	8.0
Mead	4.40	7.23	4.27	7.67
SD	0.51	0.73	0.27	0.52
Session 4				
n	20.00	20.00	6.00	6.00
Min	3.36	6.5	3.40	6.5
Max	5.48	8.0	5.32	8.0
Mean	4.39	7.18	4.28	7.25
SD	0.61	0.71	0.63	0.82

The frequency histograms of the summary data in Table 4 are illustrated in Fig. 30 to 33 for ultrasound P8 fat and numerical muscle score and 3D camera technology objective measurements.

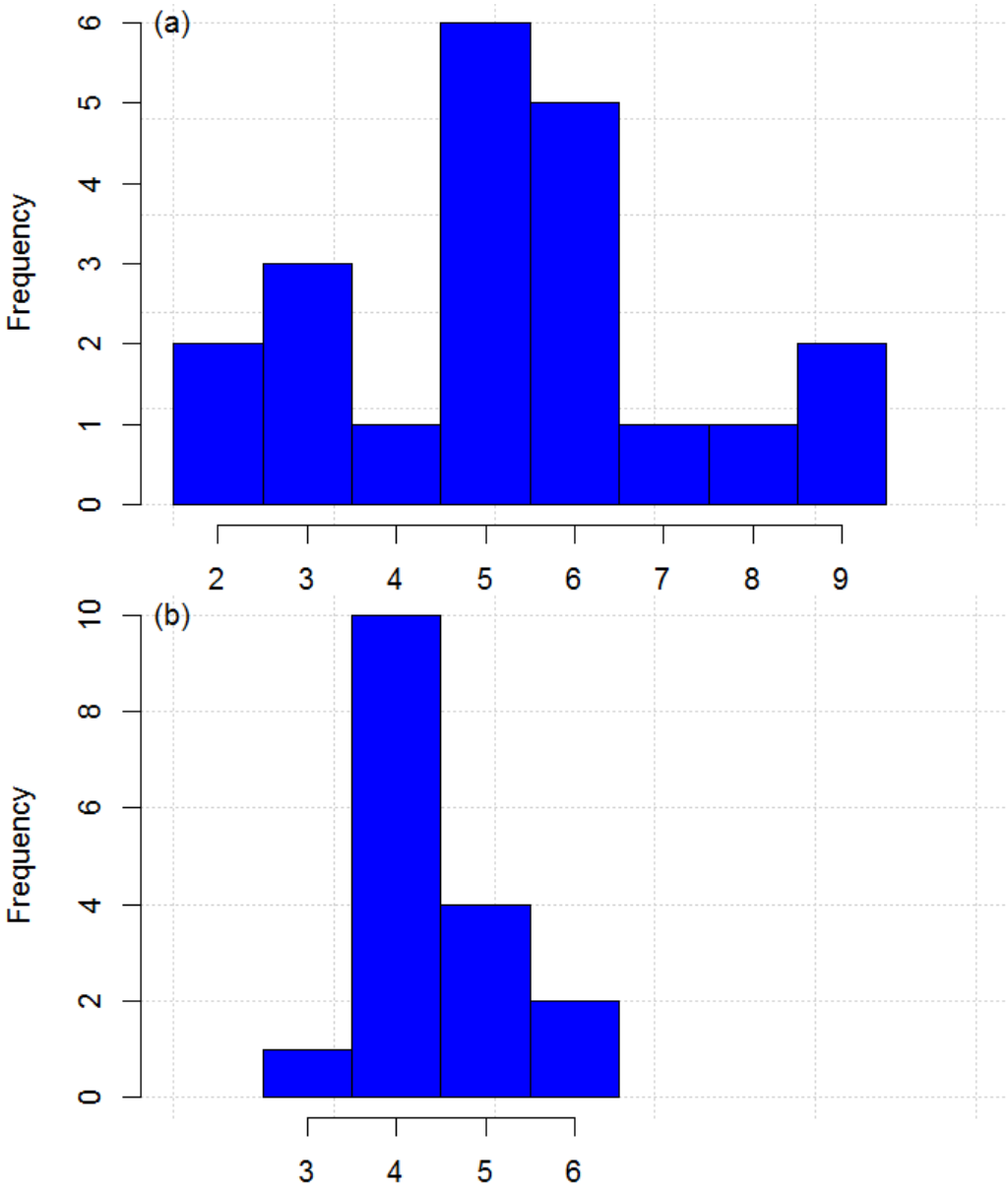

Fig. 30. Frequency histogram of heifers (a) ultrasound P8 fat (mm) and (b) 3D camera assessment of P8 fat (mm) session 1

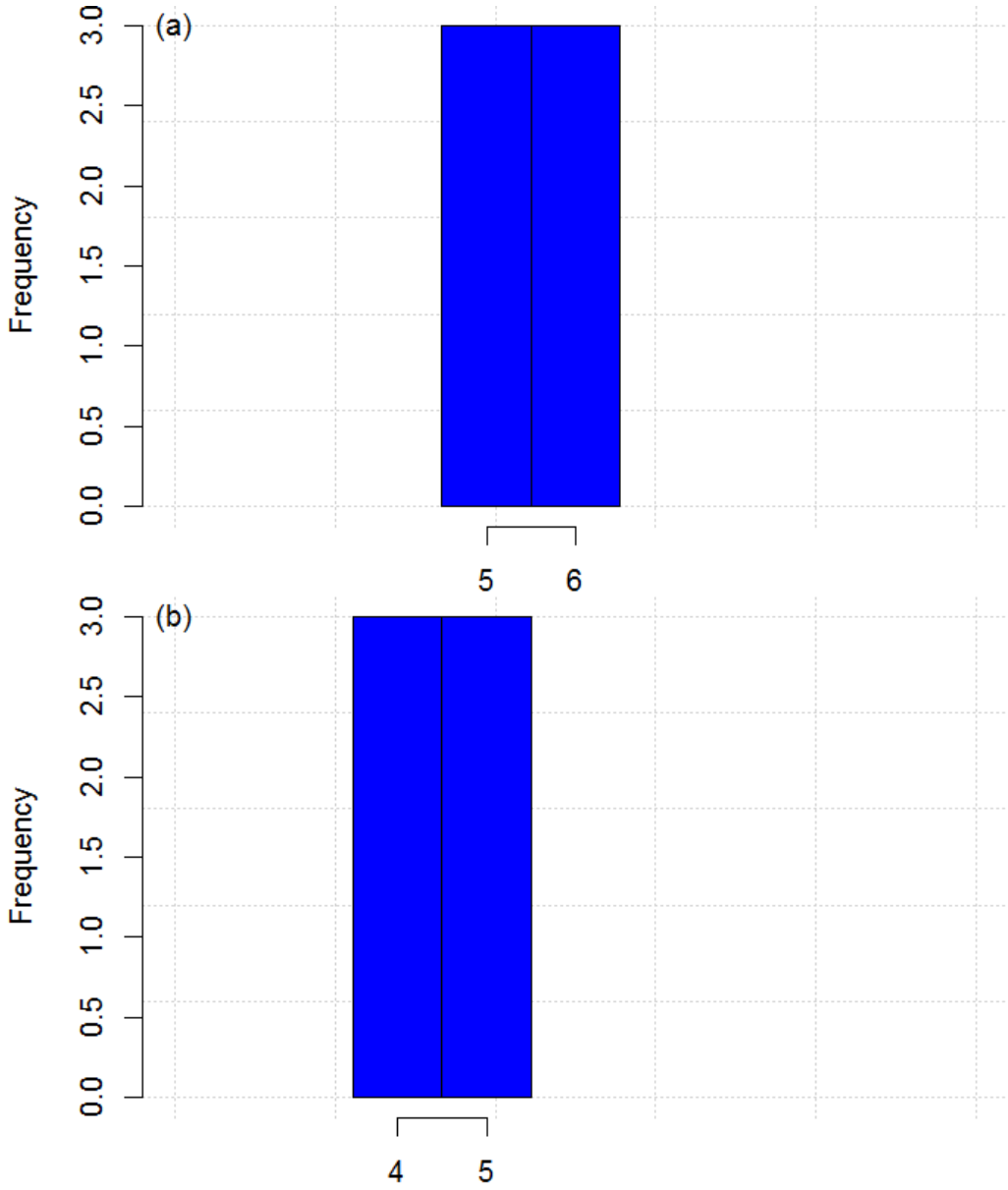

Fig. 31. Frequency histogram of steers of (a) ultrasound P8 fat (mm) and (b) 3D camera assessment of P8 fat (mm) for session 1

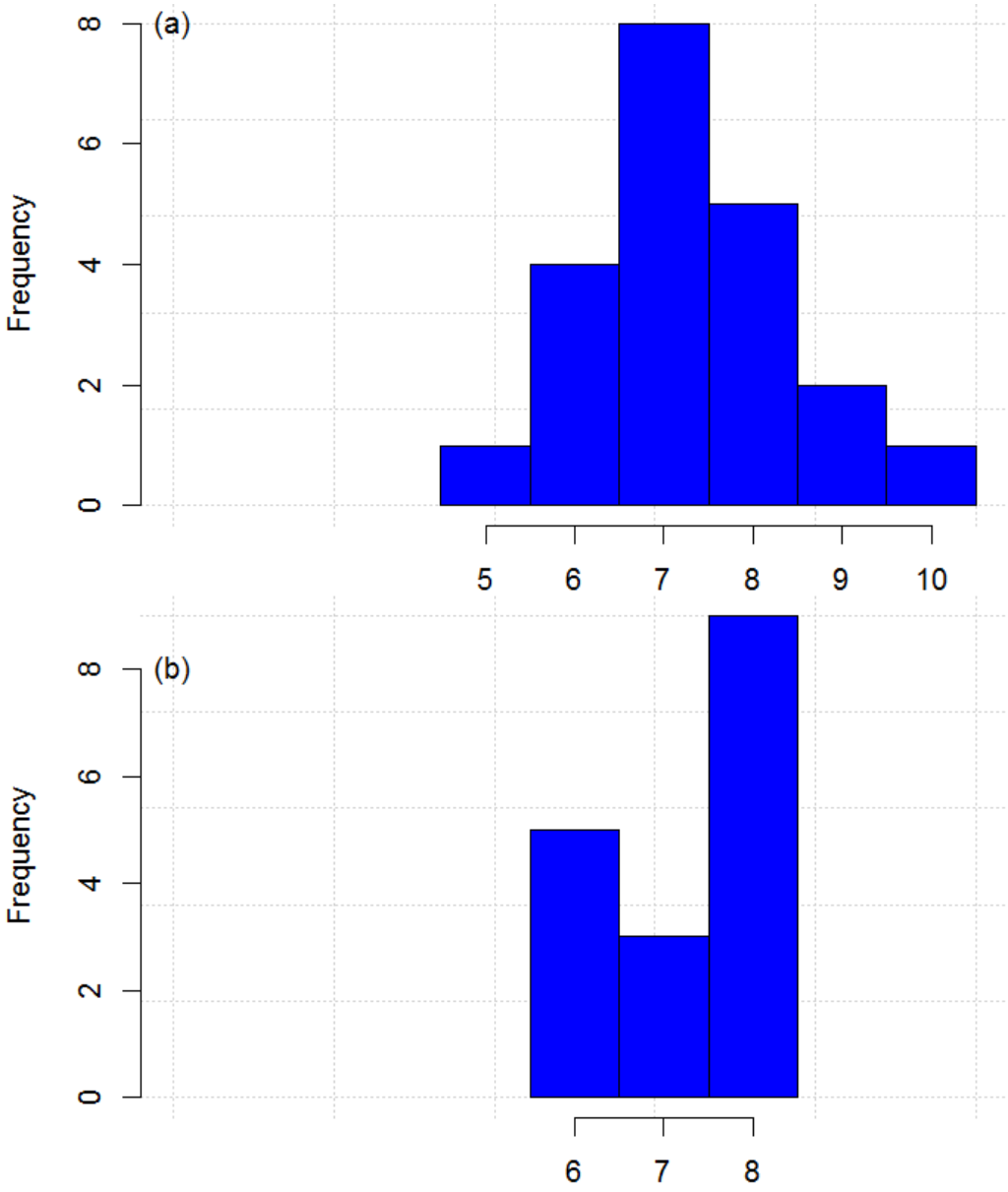

Fig. 32. Frequency histogram of heifers (a) assessed muscle score and (b) 3D camera assessment for session 1

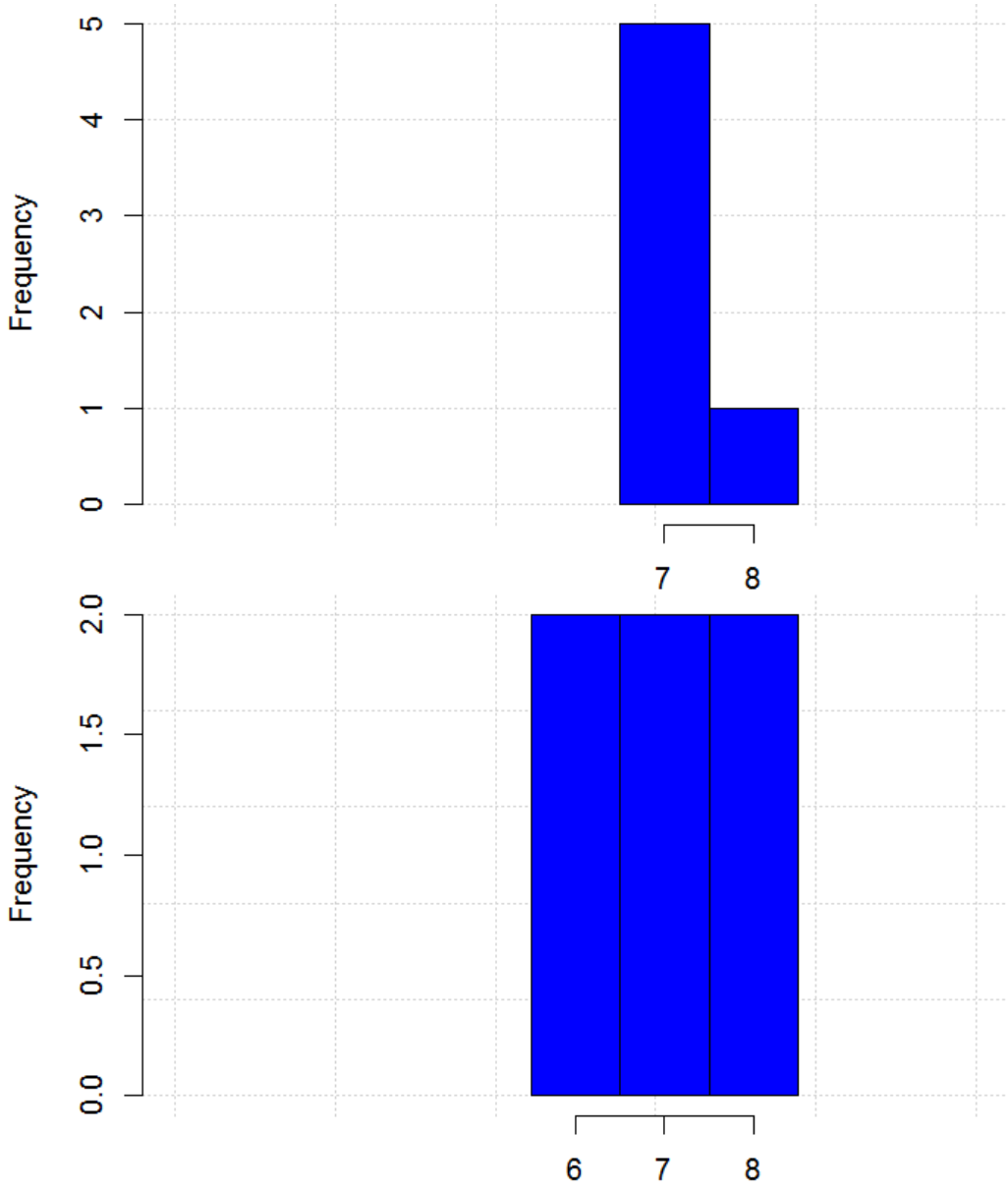

Fig. 33. Frequency histogram of steers (a) assessed muscle score and (b) 3D camera assessment for session 1

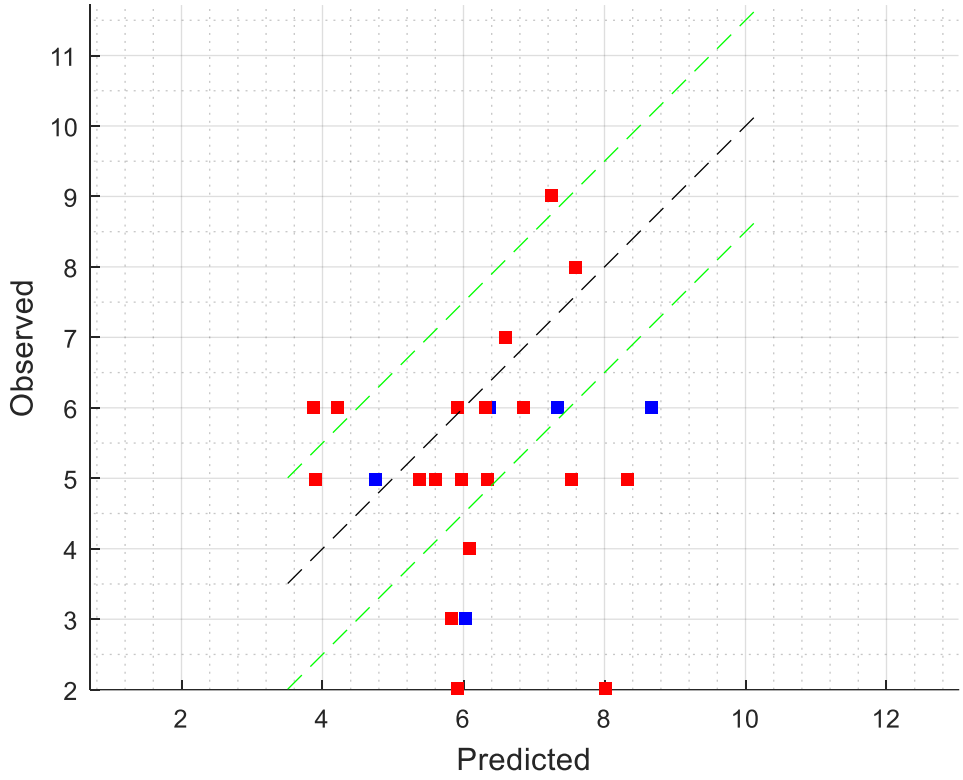

Fig. 34. Results of Tullimba 2017 (September) measured P8 fat (mm) versus assess 3D camera technology P8 fat (mm) based on model built on Tullimba 2016 data

Accuracy of assessment of Tullimba 2017 (September) muscle score for the model built on Tullimba 2016 data is reported in Table 6.

Table 6. Accuracy between the trained assessor and the 3D camera technology built on the Tullimba 2016 data and evaluated against the Tullimba 2016 data for muscle score on a 1 (D-) to 15 (A+) scale. Values along the diagonal indicate the number of times the 3D camera technology assessed muscle sore as the same score.

	Assessed 3D camera technology					
Trained assessor	D	D+	C-	C	C+	B-
D	0	0	0	0	0	0
D+	0	0	0	2	0	0
C-	1	0	1	1	1	0
C	0	0	4	4	13	0
C+	0	0	2	3	6	0
B-	0	0	0	3	1	0

Table 6. indicates that the accuracy of the 3D camera technology built on the Tullimba 2016 data and evaluated against the Tullimba 2016 data on a 15 point scale was 26% and accuracy for within 1 class bound was 71%. Assessment within 1 class is considered good.

The results of P8 fat (mm) and the 3D camera technology assessment of P8 fat with ± 1.5mm for each session are reported in Table 7.

Table 7. Percentage of P8 fat, ultrasound versus 3D camera within ± 1.5 mm for each session

	Heifer		Steer	
Session	n		n	
1	17	65	6	83
2	20	60	5	40
3	20	65	6	83
4	20	60	6	67

The results of P8 fat (mm) and the 3D camera technology assessment of P8 fat with ± 1 score for each session are reported in Table 8.

Table 8. Percentage of muscle score versus 3D camera muscle score within ± 1 score for each session

	Heifer		Steer	
Session	n		n	
1	17	76	6	83
2	20	75	5	80
3	20	70	6	100
4	20	85	6	83

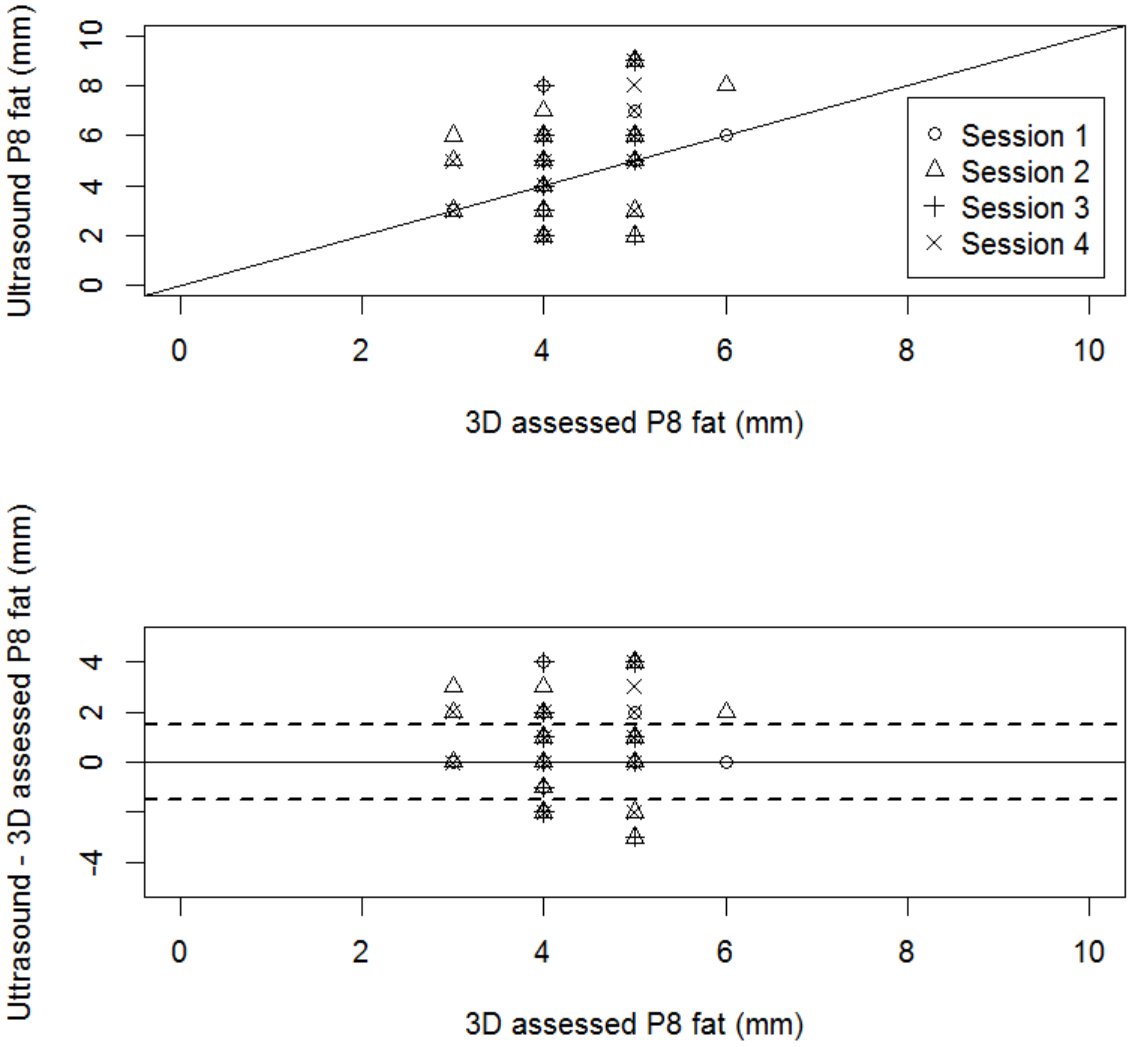

Fig. 35. Accuracy of ultrasound scanned P8 fat (mm) versus a 3D camera assessed P8 fat (rounded to a whole number i.e., integer) with a linear 1:1 line and the residuals (ultrasound scanned – 3D camera assessed P8 fat) for repeated sessions 1 to 4 (duplicates under data points). Dashed line represents ± 1.5 mm proficiency level for registered ultrasound scanners (BREEDPLAN 2016).

Figure 35 illustrates the relationship between ultrasound scanned P8 fat and the 3D camera assessed P8 fat values rounded to a whole number i.e. integer. The rounded P8 fat was then at the same level of significance (i.e. integer) as reported by assessors using an ultrasound scanner. The residuals of the difference between ultrasound and 3D assessed P8 fat were also reported indicating that 64% of the 3D camera assessed P8 fat (mm) values over 4 repeatable sessions, on the same animals, were within ± 1.5 mm within the proficiency level of a registered ultrasound scanner (BREEDPLAN 2016).

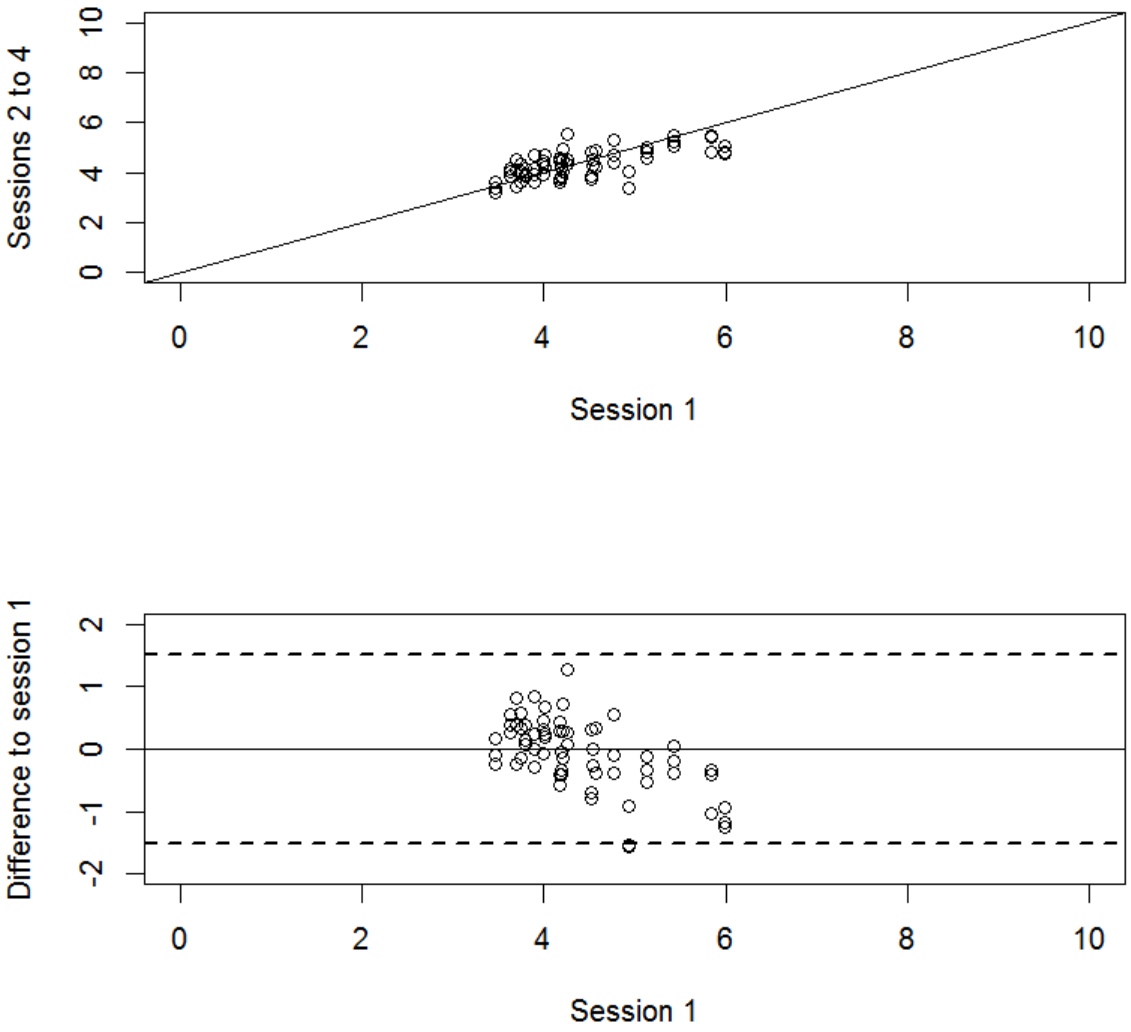

Fig. 36. Accuracy of repeatability of 3D cameras to assess P8 fat of sessions 2 to 4 versus session 1 (duplicates under data points). Dashed line represents ± 1.5 mm proficiency level for registered ultrasound scanners (BREEDPLAN 2016).

Figure 36 illustrates the relationship between the repeatable sessions 2 to 4 versus session 1 and the residuals (differences between session 2 to 4 and session 1). The residuals indicate that 97% of P8 fat over 4 sessions was within ± 1.5 mm.

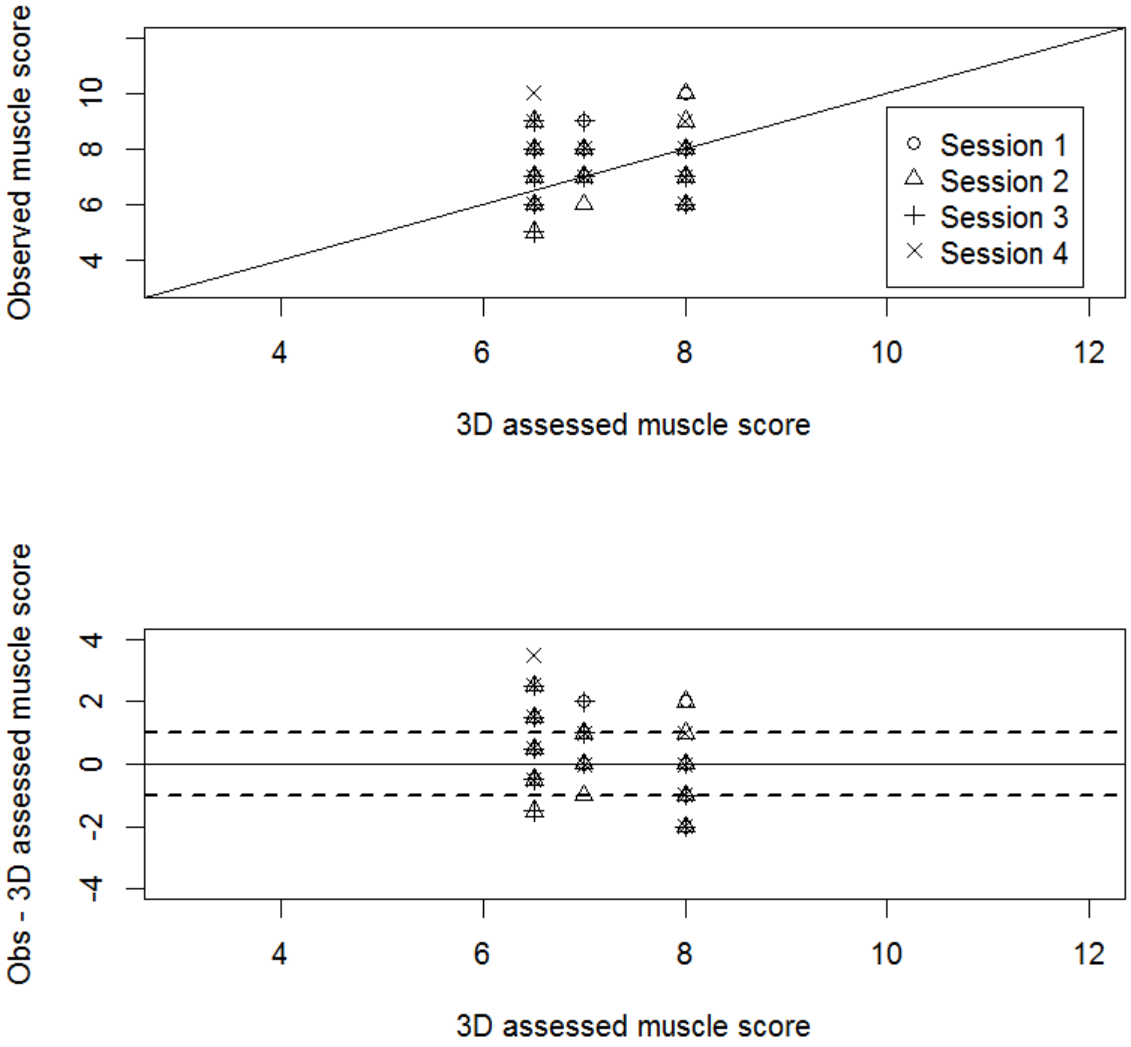

Fig. 37. Accuracy of observed muscle score versus a 3D camera assessed muscle score with a linear 1:1 line and the residuals (observed muscle score – 3D camera assessed muscle score) for repeated sessions 1 to 4 (duplicates under data points). Dashed line represents ± 1 muscle proficiency level for registered muscle scorers (AuctionsPlus p 41 and 44 2011).

Figure 37 illustrates the relationship between visually assessed muscle score and the 3D camera assessed muscle score values and the residuals of the difference between visually assessed and 3D assessed muscle score. The residuals indicate that 77% of the 3D camera assessed muscle score values over 4 repeatable sessions, on the same animals, were within ± 1 muscle score which is within the proficiency level of a good assessor (AuctionsPlus p 41 and 44 2011).

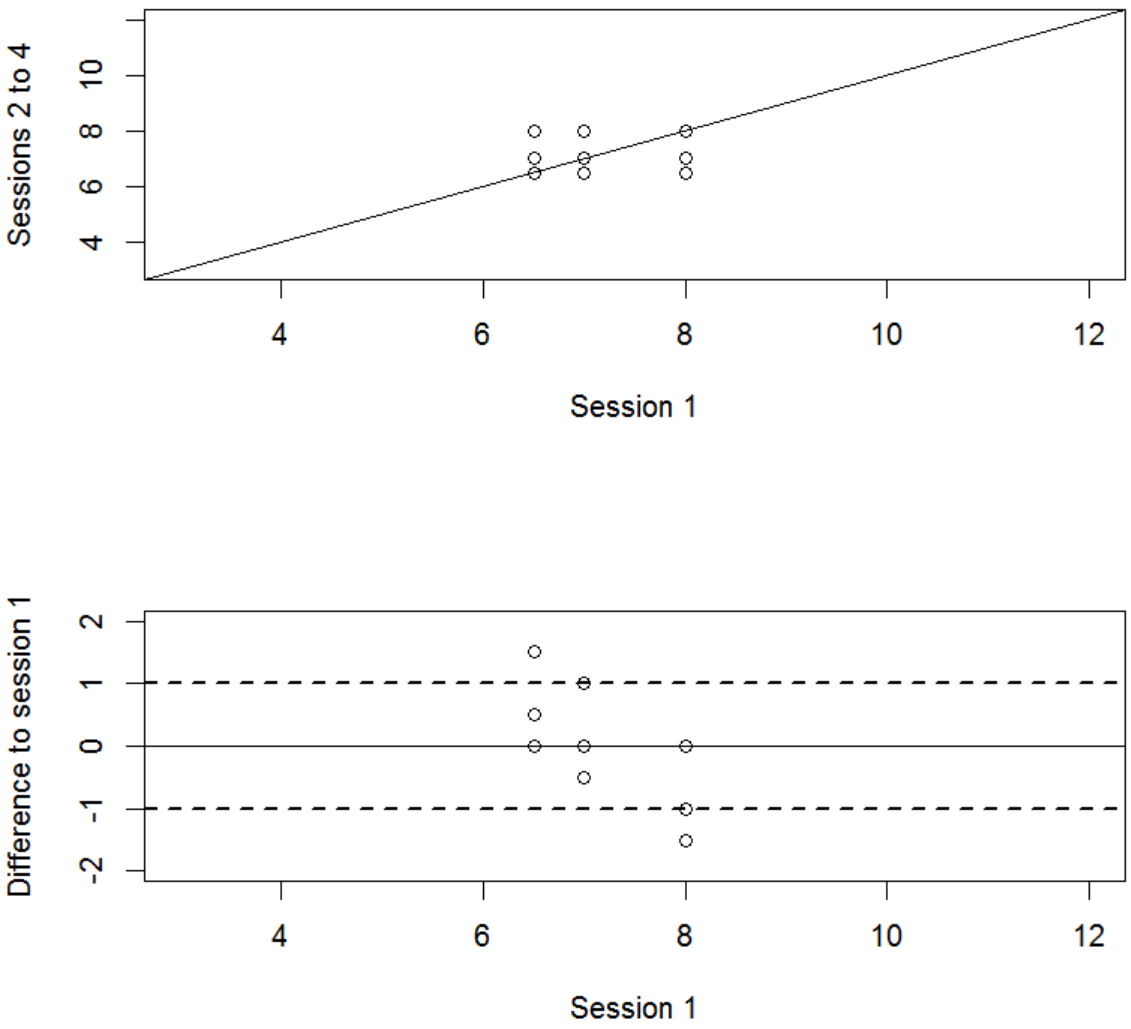

Fig. 38. Accuracy of repeatability of 3D cameras to assess muscle score of sessions 2 to 4 versus session 1 (duplicates under data points). Dashed line represents ± 1 muscle proficiency level for registered muscle scorers (Auctions Plus 2011; p 41 and 44).

Figure 38 illustrates the relationship between the repeatable sessions 2 to 4 versus session 1 and the residuals (differences between session 2 to 4 and session 1). The residuals indicate that 80% of 3D assessed muscle scores, over 4 sessions, were within ± 1 muscle score.

5 Discussion

This project has successfully delivered on a number of the objectives and identified weakness where improvements need to be made. The development of a real-time objective measurement of hip height, P8 fat, and muscle score is a significant achievement. The 3D camera technology being developed has the potential to revolutionize the beef industry. The integration of the 3D camera system with the BeefSpecs will assist producers improve market specifications and hence assist the beef industry move towards a value based trading system. The new enhanced BeefSpecs also has the potential to play a significant role in assessing lean meat yield on live cattle that will assist producers make management decisions before slaughter. The following sections highlight where further improvements are required and also provide a summary of the achievements achieved for each of the project objectives.

5.1 Trait Estimation System Using Curvatures

The current trait estimation framework leverages surface curvatures for both P8 and muscle score estimation. While the majority of the results obtained by the system are within the bounds acceptable for a certified ultrasound operator (1.5mm) and assessor (one class on a 15 class scale), the system is overestimating animals with low P8 fat and muscle score values. While the muscle score estimation errors can be attributed to the under representation of low muscle scored animals (D- and below) this is not evident as primary reason of low P8 fat estimates, the origins of these errors are significantly more complex. In particular, the 10 fold cross validation on the Tullimba dataset demonstrates that within the same cohort used for building the model there is clear underestimation of P8. Analysis performed indicates this can be attributed to three main reasons: (a) tail removal as part of processing; (b) susceptibility to orientation and neutral pose errors; (c) machine learning framework not penalising overestimation; and finally gender related bias is not completely ruled out.

5.1.1 Tail removal problems

Multiple acquired frames (at present 8) are used to achieve estimation in order to ensure the underlying point cloud representation is sufficiently dense to achieve estimation and resilient to both glare from the environment and sensor noise. During this process, removal of the tail of the animal occurs, a trade-off between speed (complexity) of this process and sufficient data of the rear of the animal is undertaken. At present, the rear of the animal is detected and all points within 10cm of the rear of animal are removed, followed by removal of any other non-connected points. This does leave the bulk of the animal visible, with the pin bone area sacrificed for simplicity of the pipeline. While this area could be intuitively seen as irrelevant to the muscle score estimation, it does play a part in P8 fat (mm) assessment, as the area of the pin bones is filled with subcutaneous fat deposition.

5.1.2 Susceptibility to orientation and neutral pose

As 3D images acquired in the chute, leaner animals have more of a capacity to move sideways and skew their appearance. A demonstration of the difference in acquired images of a leaner and more “rounded” animal as can be seen in Fig. 38, view over the stifle are not completely available, there

are regions with no acquired data, therefore the estimation framework is unable to produce a reliable result.

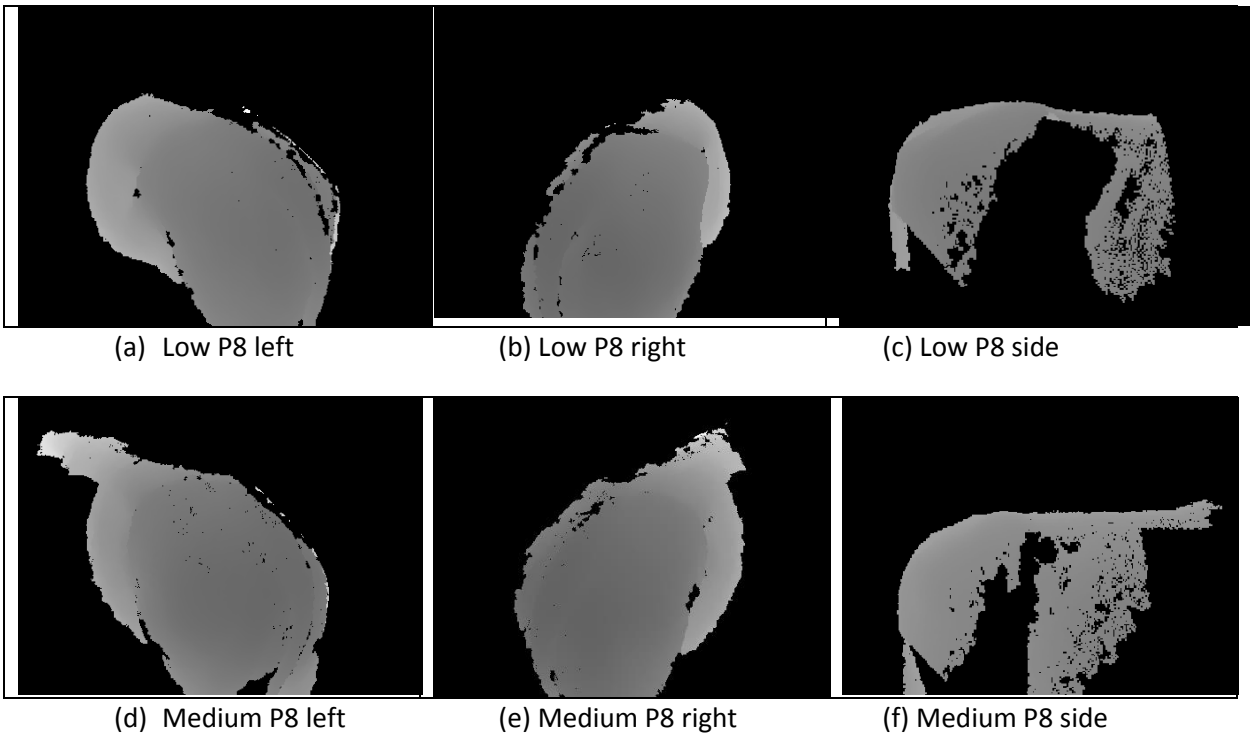

(a) Low P8 left (b) Low P8 right (c) Low P8 side

(d) Medium P8 left (e) Medium P8 right (f) Medium P8 side

Fig. 38. Acquired data of animal with low P8 fat (top row) and medium P8 fat animal (bottom row). The rump length appears the same, however the stifle width obstructs more of the area of the animal visible to the 3D camera on low fat animal (comparison between (c) and (f) views).

5.1.3 Model development

The model development phase in this project is based on the largest sample acquired (Tullimba 2016) with the largest variation of Muscle Score and P8 Fat values. While the majority of this data is sufficient quality, there have been vast improvements in the automation framework as well as the chute development. From Inverell 2016 (proto type testing) the GUBE is used to estimate the appropriate camera placement (race configuration) and effects of lighting. A new enclosure of chute has increased the reliability of the data, as demonstrated in Fig 39.

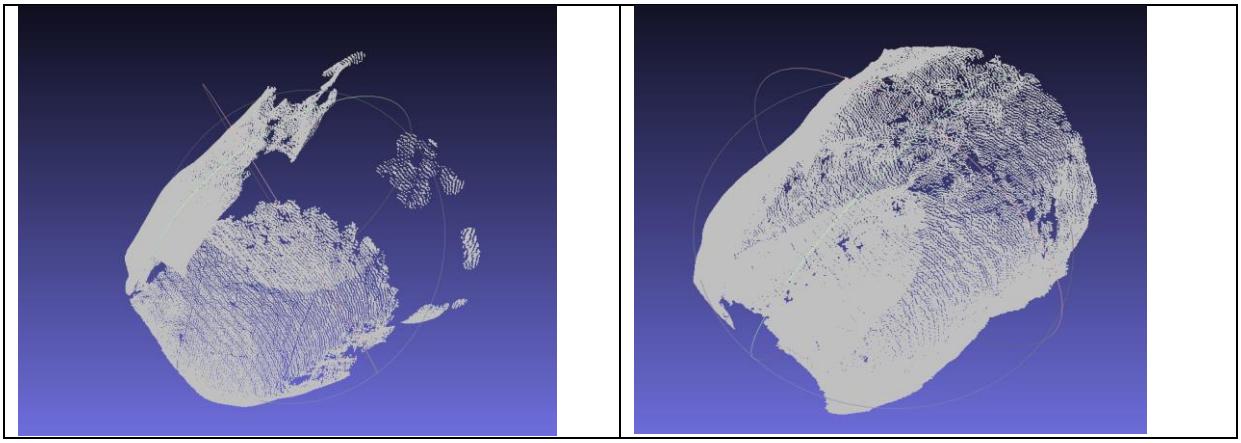

Fig. 39. Difference in acquired data due camera setup with respect to race configuration and light leakage (a) Tullimba 2016 / 10 (Trained Dataset), data with missing sections due to poor race configuration (b) Tullimba 2017 / 09 (Test Dataset) with complete data and race configuration improvements

Further, at present the models to be used for any subsequent estimation, as derived from the 10 fold cross validation scheme using the Gaussian Process, are selected based on the RMSE as well as convergence properties of the Gaussian Process. The model development and validation are truly random, whereas a scheme that could select better representative groups across all animals available could yield a better overall performance. A metric to reject samples from being included in the, which would in effect require a semi-supervised or unsupervised machine learning approach, as opposed to current supervised approach.

5.2 Summary of achievements for project objectives

5.2.1 Determine configuration of cameras and simple calibration procedures

A light weight auto-calibration apparatus called the “GUBE” was developed. The GUBE is a simple calibration procedure which is much more robust and efficient compared to the previous calibration apparatus. Further research is still required to find a way to detect the change in camera position due to the animal/human disturbing the configuration.

5.2.2 Animal stance design to allow developing adequate 3D model capture and practicality for deployment in field. This includes animals standing on a weighing platform.

A description of the processes: stability detection and segmentation, and point cloud reorientation through spline localisation to detect stability have been described. Detection of stability is generally found within 1 minute and visually displays a green coloured in image indicating that the reporting of hip height, P8 fat (mm) and muscle score was to follow.

5.2.3 Develop the data framework for in-situ extraction 3D body representation related to gross body shape, through curvatures

The demo trial at the Tullimba feedlot in September 2016 clearly demonstrated that software has been extensively developed to perform the feature extraction and assessment of P8 fat and muscle

score from machine learning. There are several underlying issues that contribute to the fragility of the alternative feature vectors: (i) bending energy and (ii) hjorth activity of the surface that were analysed. The issues are related to alignment, scaling where the distance from one's pin bone to hip is different to another animal and misalignment. Future work will endeavour to resolve these alignment issues, which are fundamental in ensuing the robustness of any feature vector based on geometric information such as is available in the consolidated point clouds in the current data set.

5.2.4 Develop the supporting machine learning framework to produce trait estimates

Several studies within this project used independent data (i.e., data not seen before by the 3D cameras). When assessing P8 fat we found that errors existed in either low or high values. In order to improve this assessment of P8 fat at lower and higher values several steps were put into place. One of these was the development of 2 alternative feature vectors the bending energy and the hjorth activity and the other approach was the use of Convolution Neural Networks (ConvNet/CNN's). Both of these approaches have been very fruitful in improving the overall assessment of P8 fat at lower and higher P8 fat values in the 2 to 11 mm range. In particular, the ConvNet has improved the assessment of the P8 fat at the higher range. Further work is required to determine why the lower values have been more difficult to assess. Needless to say that data availability is one issue (see frequency histograms) and secondly statistical models generally have larger confidence intervals around the lower or upper ends of a relationship.

5.2.5 Design, plan and construct a prototype chute.

A new prototype measurement chute with extensive shading to reduce direct sunlight on the area where 3D images are taken has been implemented. The improve prototype chute has improved the clarity of images and hence the quality of data collected has increased.

5.2.6 Conduct two trials at feedlots using the 3D camera system to assess in situ muscle score, hip height and P8 fat

Two trials were conducted on cattle that had not been seen by the cameras. These trials were very fruitful in providing data to determine where weaknesses either existed in the measurement chute or in the accuracy of assessment.

6 Conclusions/recommendations

This project builds upon research work carried out in the 'proof of concept' (B.BSC. 0339) study supported by MLA concerning trait assessment using RGBD camera technology. Specifically, this project extends the research already conducted using 3D images for assessing live animal P8 fat (mm) and muscle score in the NSW DPI Glen Innes low and high muscling Angus herd. While the focus of earlier work in estimating live animal traits that allows forward prediction of lean meat yield (LMY) *via* tools developed within the Beef CRC (i.e., BeefSpecs). Extension work undertaken within ALMTech (RnD4Profit-15-02-03 'Advanced measurement technologies for globally competitive Australian meat value chains') will determine the capacity of the 3D imaging system to be breed agnostic (beyond Angus) and directly predict LMY of cattle within 10 days of slaughter. The later goal specifically averages the collection of LMY data post slaughter undertaken within the ALMTech program.

The approach using 3D cameras attempts to exploit changes to body shape in response to *subcutaneous fat deposition* and building of muscle that is visible on surface as gross curvature. The patterns of shape/curvature and relationship to underlying trait are established via a machine learning framework, a common approach to establish relationships between multidimensional data and a specific value, where no underlying physical model can be established. Differences in shape between the Bos Indicus, Bos Taurus and European cattle indicate existing models built for Bos Taurus (specifically Angus) cattle would not transpire across to other species. Further work is therefore required to exploit other breeds. Additional work on improving the accuracy of assessing P8 fat and muscle score at the lower P8 fat assessments is also required along with a larger repeatability study.

Predictions of LMY, MSA marbling, and MSA index on live animals developed from a serial slaughter study on Angus cattle from weaning to slaughter in the enhanced BeefSpecs (B.BSP.00111) project needs validating. This validation can be achieved by value adding to the ALMTech project through accessing cattle from weaning to slaughter that will be assessed by the DEXA.

Case studies using the 3D camera technology and the BeefSpecs tools will provide an avenue to show case this technology and extend this to industry. The 3D camera technology has the potential to make a large impact on the red meat industry by providing objective measurements on live cattle that reduces the variation between assessors and provides a way of reporting traits (i.e. muscle score) that otherwise would not be known because of time constraints, costs and skills that are required to obtain these assessments.

7 Key messages

The objective measurements on live cattle provides an opportunity for producers to make on-farm management decisions to improve profitability by being involved in the feedback loop from weaning through to slaughter from paddock to plate. The economic benefits to producers include: increase in market compliance, improvements in LMY, MSA marbling, and MSA index. The 3D technology reduces variability between assessors and provides objective data that would otherwise be very difficult and cost prohibitive to obtain.

8 Bibliography

Bishop CM, (2006) Pattern Recognition and Machine Learning. Springer, New York.

Hubel HD, Wiesel TN (1959) Receptive Fields of Single neurons in the Cat's Striate Cortex. *Journal of Physiology*. **148**, 574-591.

Krizhevsky A, Sutskever I, Hinton GE (2012) ImageNet Classification with Deep Convolutional Neural Networks. Advances in Neural Information Processing Systems. Vol 25.

LeCun Y, Bottou L, Bengio Y, Haffner P (1998) Gradient-based Learning Applied to Document Recognition. In 'Proceedings of IEEE November 1998'. Vol 86, pp. 2278–2324.

McPhee MJ, Walmsley BJ, Skinner B, Littler B, Siddell JP, Cafe LM, Wilkins JF, Oddy VH, Alempijevic A (2017) Live animal assessments of rump fat and muscle score in Angus cows and steers using 3-dimensional imaging. *Journal of Animal Science* **95**, 1847-1857.

Murphy K P (2012) Machine Learning: A Probabilistic Perspective. Cambridge, Massachusetts: The MIT Press.

Nagi J, Ducatelle F, Di Caro GA, Ciresan D, Meier U, Giusti A, Nagi F, Schmidhuber J, Gambardella LM (2011) Max-Pooling Convolutional Neural Networks for Vision-based Hand Gesture Recognition. In 'Proceedings of IEEE International Conference on Signal and Image Processing Applications 2011'.

Nair V, Hinton GE (2010) Rectified linear units improve restricted Boltzmann machines. In 'Proceedings of 27th International Conference on Machine Learning'.

Srivastava N, Hinton G, Krizhevsky A, Sutskever I, Salakhutdinov R (2014) Dropout: A Simple Way to Prevent Neural Networks from Overfitting. *Journal of Machine Learning Research*. **15**, 1929-1958.